STRESSES AND FAILURE MODES IN THIN FILMS AND MULTILAYERS

Technical University of Denmark
NOTES FOR A DCAMM COURSE
October 1996
by

John W. Hutchinson
Division of Engineering and Applied Sciences
Harvard University
Cambridge, MA 02138, USA

Contents

STRESSES AND FAILURE MODES IN THIN FILMS AND MULTILAYERS

1. AN OVERVIEW

Thin films and multilayers are widely used in technology, and their mechanical performance under severe environmental conditions often dictates design. Examples include electronic packages, coatings for thermal, chemical or abrasion protection, and ferroelectric actuators. This set of notes addresses both the origins and details of the stresses which develop in thin films and multilayers and the failure modes stemming from these stresses. The notes draw from many sources in the literature but two articles, in particular, are used. An overview article (Evans and Hutchinson, 1995) provides an integrated picture of the subject which goes beyond the scope of the notes. Much of the quantitative mechanics, which will be the focus of the notes, is contained in the article by Hutchinson and Suo (1992). Specific sections from these papers will be cited and integrated into the notes as part of the reading. These two articles have an extensive list of references, which serve these notes as well. Detailed citations to the literature are not provided in these notes.

1.1 Stresses: Origins and Terminology

Stresses in thin films and multilayers have three primary origins: *intrinsic*, *thermal* and *mechanical*. Intrinsic and thermal stresses are often referred to as *residual stresses*. Stresses which arise from mechanical (as opposed to thermal) loads are labeled "mechanical stresses" for the present discussion.

Intrinsic stresses arise during the deposition process, which include sputtering, spraying, painting, spin coating, vapor deposition, and electro–deposition. These processes are used to create films and multilayers from metals, ceramics, polymers and intermetallics. Depending on the process, the deposition temperature can be "low" or "high" or room temperature. Intrinsic stresses are distinct from thermal stresses in that they are the stresses present at the deposition temperature. The mechanisms which generate intrinsic stresses are not well characterized quantitatively. They include grain growth, defect annihilation, phase transition, and evaporation of a solvent. For example, vacancy annihilation would reduce volume were a film free to contract. Thus, a film on a substrate would develop intrinsic tensile stress if it experienced vacancy annihilation.

When a single crystal thin film is deposited *epitaxially* on a single crystal substrate (one perfect atomic lattice on top of another), there will usually be an intrinsic stress in the film due to the difference between the unstrained lattice spacings of the film and substrate materials.

Thermal stresses arise due to changes in temperature when the film and substrate (or the layers in a multilayer) have different coefficients of thermal expansion (CTE). For some systems, these stresses can be huge (i.e. several GPa), and they are frequently provide the driving force for mechanical failure.

When the temperature is different from the deposition temperature, the residual stresses comprise both intrinsic and thermal contributions.

1.2 Failure Modes: An Overview

There are many modes of failure of films and multilayers which result from stresses which are too large. Interfaces are intrinsic to these systems, and they are susceptible to interface debonding or delamination. Cracking of a film or layer is possible when tensile stresses develop, while buckling–driven delamination can occur if stresses are compressive.

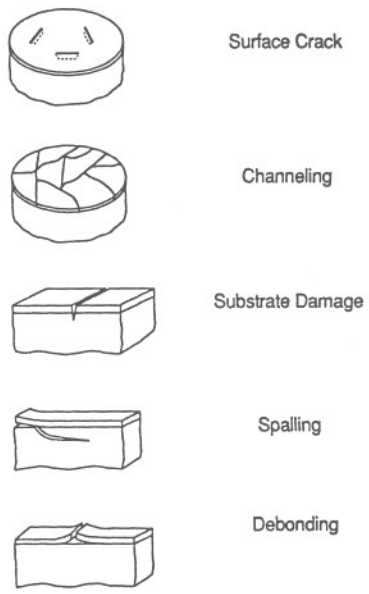

Fig. 1.1. Cracking modes in films stressed in tension.

Several modes of cracking are depicted in Fig. 1.1 for a film on a substrate where the *film is in tension*. Isolated surface cracks can propagate and channel across the film. If the substrate is brittle the crack may penetrate into the substrate, even though it is essentially unstressed. The interface may debond, or a debond crack may dive into the substrate producing delamination via cracking parallel to the interface in the substrate. Combined film cracking and interface debonding can also take place if the combination of film toughness and interface toughness lies within certain limits.

Each of the lower four modes shown in Fig. 1.1 involves *steady–state propagation* once it has advanced beyond a distance typically on the order of the film thickness. These steady–state propagation modes will be analysed later in the notes for both films and multilayers.

Although the modes are 3 dimensional, they can be analysed with 2D solutions. They provide robust fail–safe criteria for ensuring that the respective failure modes will not occur. The combination of parameters which form the criteria always has the nondimensional form

$$\Omega = \frac{h\sigma^2}{E\Gamma} \tag{1.1}$$

where h is a film or layer thickness, σ a stress, E a modulus, and Γ a toughness (in units Jm^{-2}) . If the "cracking number", Ω , is less than a critical value, Ω_C (depending on the specific mode), the mode is excluded. Thus, for example, film debonding (Fig. 1.1) is excluded if $\Omega < 2$, where h is the film thickness, σ the film stress, E is the plane strain tensile modulus, and Γ is the interface toughness.

When the stress in the *film is compressive*, there are two dominant failure modes: buckling–driven interface delamination and edge delamination, as depicted in Fig. 1.2. The shapes and propagation patterns of the buckle delamination modes can be quite extraordinary. These modes are also characterized by criteria which can be expressed in the form (1.1).

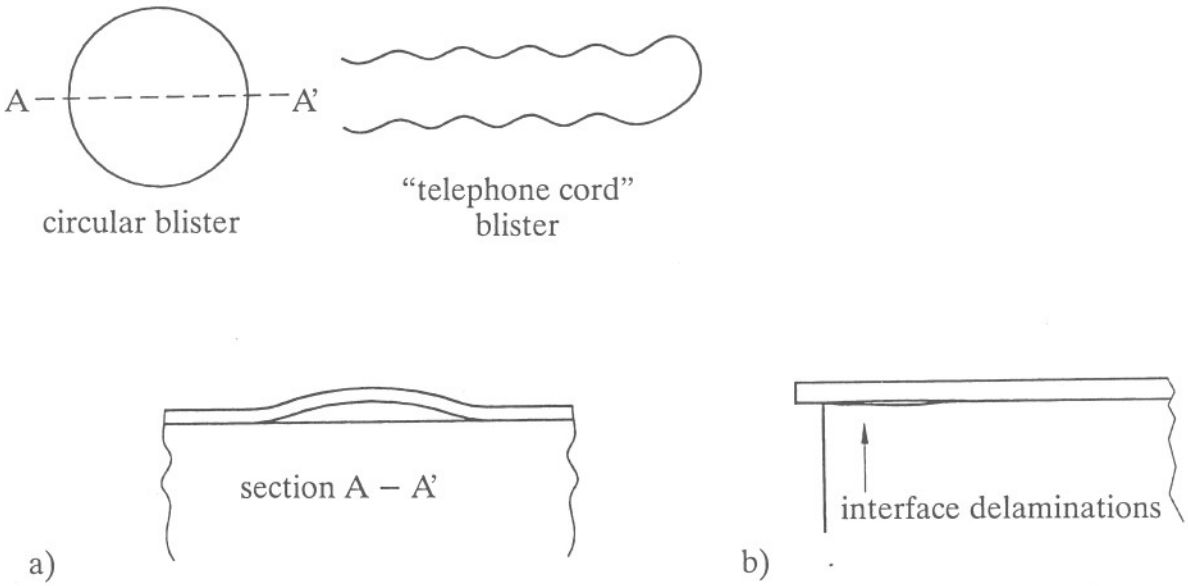

Fig. 1.2. Failure modes for compressed films. (a) Buckling driven interface delamination, and (b) Edge delamination.

Internal layers of a multilayer can undergo cracking and interface debonding, and in combination when the ratio of the toughnesses of the layer and interface is between certain limits. Fig. 1.3 depicts a tunnel crack propagating in a layer accompanied by interface debonding and sliding.

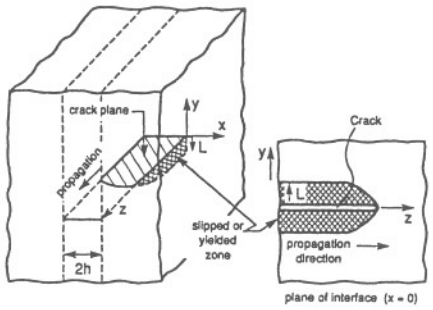

Fig. 1.3. A schematic of crack growth in a multilayer by tunnelling with slip or debonding at the interfaces.

Interfaces are inherent to thin films and multilayers. There are critical issues which influence the integrity of the system. Will an interface crack propagate? Or will it kink into an adjoining layer? Will a crack intersecting an interface pass through or will it be deflected into the interface? Interface toughness and its magnitude relative to that of adjoining layers is central to the answers to these questions.

Plasticity accompanying crack growth can have a major influence. In most instances plasticity increases the resistance to crack growth. However there are certain problems for films and layers where plasticity enhances crack propagation. The first sections of the notes address behavior from the vantage of elastic crack mechanics. Some of the issues surrounding the role of plastic deformation in films, substrates and layers are taken up in the final sections.

2. STRESSES IN FILMS AND MULTILAYERS

2.1 Intrinsic Stresses

As mentioned in Section 1.1, intrinsic stresses are defined to be those stresses which arise during the deposition process which are not due to thermal expansion mismatches. Most mechanisms generating intrinsic stress result in a change in volume which then produce stresses due to the constraint of the substrate or other layers. The mechanisms are not well quantified and most estimates of intrinsic stress levels are obtained by experimental measurement. Several models for mechanisms which give rise to tensile stresses in thin film deposition are presented in the Appendix of the paper by Evans and Hutchinson (1995). These include grain growth, defect annihilation and sintering.

2.2 Thermal Stresses in a Thin Film

To fix some of the ideas and notation, consider a very thin film on a thick substrate $(h/H << 1)$, as shown in Fig. 2.1. The film and substrate are each isotropic with (E, ν, α) and (E_s, ν_s, α_s) as the respective Young's modulus, Poisson's ratio and CTE.

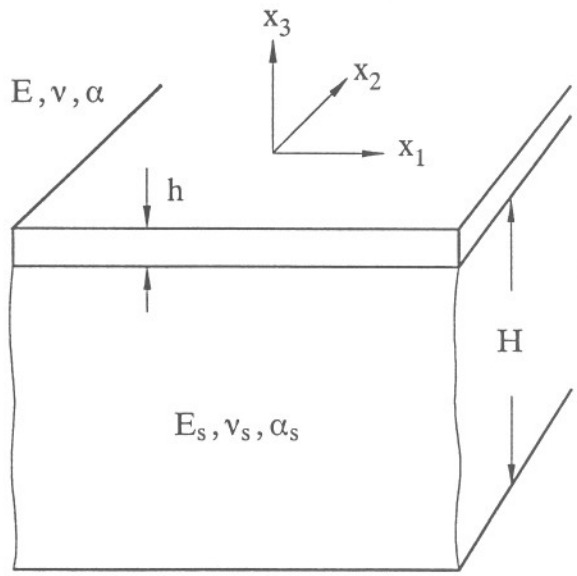

Fig. 2.1. Thin film on a thick substrate.

Attention is directed first to stresses which develop in the *interior of the film* away from the edges. The film is deposited at temperature T_0 with intrinsic stresses $\sigma_{11} = \sigma_{22} = \sigma^I$, which may very with x_3. Assuming an *elastic* response, consider the effect of changing temperature from T_0 to T with $\Delta T = T - T_0$. Let $\Delta\sigma_{ij}$ be the associated stress changes (i.e. the thermal stresses) such that the total stress at T will be $\sigma_{ij} = \sigma^I_{ij} + \Delta\sigma_{ij}$. Let ϵ_{ij} be the strains measured relative to the state at T_0. For $h/H << 1$, the film has little effect on the substrate and the substrate imposes its *inplane strains* on the film. Thus, away from the edges,

$$\left(\epsilon_{\alpha\beta}\right)_{\text{film}} = \left(\epsilon_{\alpha\beta}\right)_{\text{substrate}} \qquad \alpha = 1,2\ ;\ \beta = 1,2 \tag{2.1}$$

There is no bending. The substrate expands freely, effectively uninfluenced by the film. In the next section, the effect of interaction between film and substrate with finite h/H will be analysed accounting for bending.

By (2.1), for both the film and substrate

$$\epsilon_{\alpha\beta} = \alpha_s \Delta T \delta_{\alpha\beta} \qquad \alpha = 1,2\ ;\ \beta = 1,2 \tag{2.2}$$

(This is valid if α_s is independent of T. If α_s depends on T, then $\alpha_s \Delta T$ should be replaced by

$$\int_{T_0}^{T} \alpha_s \, dT$$

Equivalently, (2.2) holds rigoriusly if α_s is taken as the average of the CTE on the interval T_0 to T) . The component ϵ_{33} in the film is unconstrained and $\sigma_{33} = 0$, corresponding to plane stress conditions. The inplane components ($\alpha = 1,2$; $\beta = 1,2$) in the film satisfy

$$\epsilon_{\alpha\beta} = \frac{1+\nu}{E}\Delta\sigma_{\alpha\beta} - \frac{\nu}{E}\Delta\sigma_{\gamma\gamma}\delta_{\alpha\beta} + \alpha\Delta T\delta_{\alpha\beta} \tag{2.3}$$

with inverse

$$\Delta\sigma_{\alpha\beta} = \frac{E}{1-\nu^2}\left[(1-\nu)\epsilon_{\alpha\beta} + \nu\epsilon_{\gamma\gamma}\delta_{\alpha\beta}\right] - \frac{E\alpha\Delta T}{1-\nu}\delta_{\alpha\beta} \tag{2.4}$$

Imposition of (2.2) gives the thermal stresses in the film away from the edges

$$\Delta\sigma_{\alpha\beta} = \frac{E\Delta\alpha\Delta T}{1-\nu}\delta_{\alpha\beta} \quad , \quad \Delta\sigma_{33} = 0 \tag{2.5}$$

where the CTE mismatch is $\Delta\alpha \equiv \alpha_s - \alpha$. (Again, note that (2.5) is rigorous for temperature dependent CTE's if $\Delta\alpha$ is taken to be the average on the interval T_0 to T) .

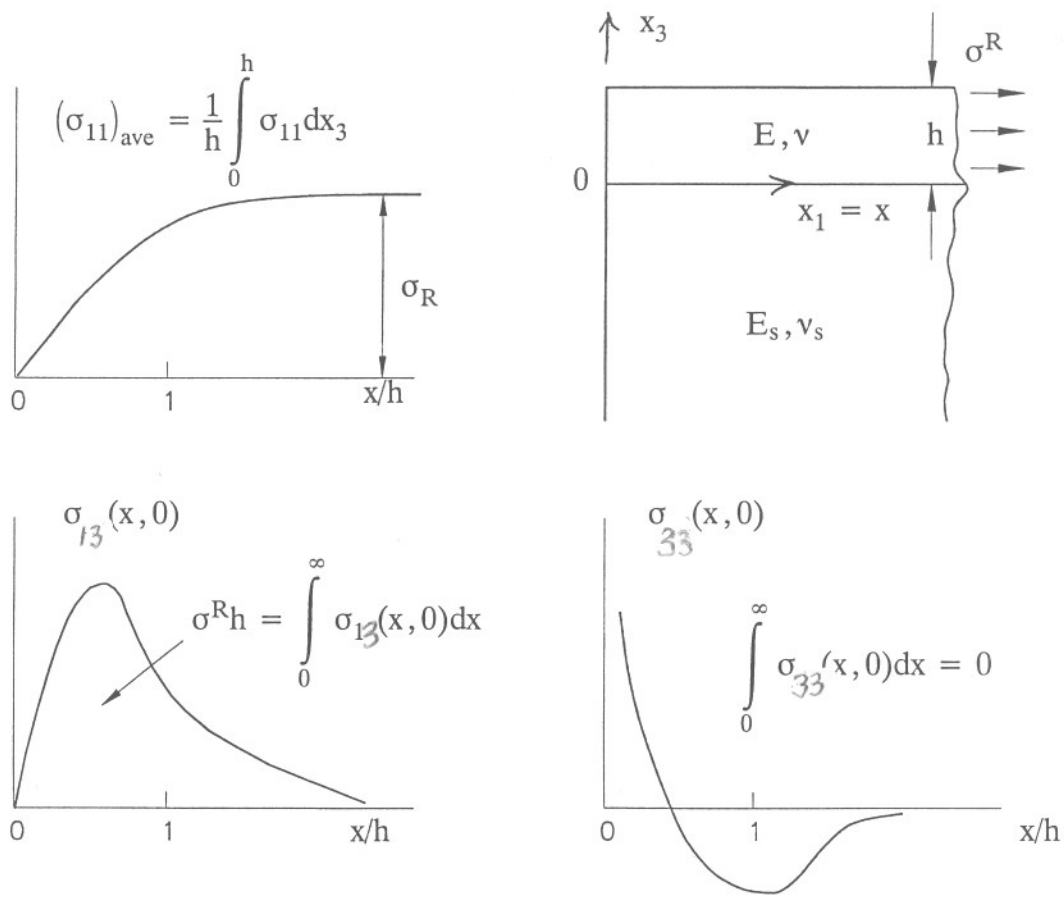

Fig. 2.2. Qualitative behavior of stresses near the edge of a thin film (away from the corners). $(\sigma_{11}(x,x_3))_{ave} = h^{-1}\int_0^h \sigma_{11}dx_3$ is the average through the thickness at $x \equiv x_1$. $\sigma_{12}(x,0)$ and $\sigma_{22}(x,0)$ are the traction components on the interface at x .

In summary, the interior of the film is subject to the equi–biaxial inplane stress state

$$\sigma^R = \sigma^I + \frac{E\Delta\alpha\Delta T}{1-\nu} \tag{2.6}$$

Closed form results for stresses near the edges or corners of the film are not available. The qualitative behaviour near an edge of a thin film (away from the corners) is sketched in Fig. 2.2. In general, the stress state may be singular at $(0,0)$ if $E_s \neq E$.

An approximate analysis of the shear traction on the interface by Freund and Hu (1988) results in the normalized results presented in Fig. 2.3. The parameter λ is given by

$$\lambda = \frac{E_s(1-\nu^2)}{E(1-\nu_s^2)} \tag{2.7}$$

Thus, if the substrate is stiff compared to the film $(\lambda >> 1)$, the shear transfer zone is narrow and on the order of h. Conversely, if the substrate is relatively compliant, the shear transfer zone is wide.

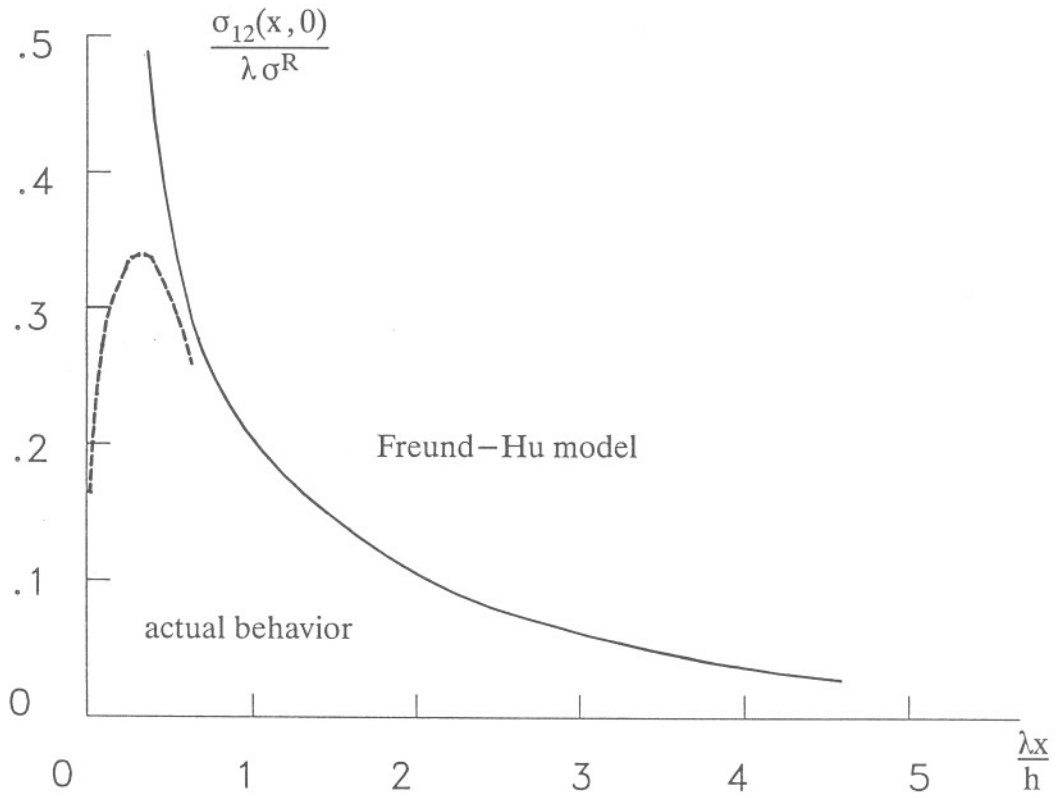

Fig. 2.3. Shear traction $\sigma_{12}(x,0)$ on the interface near the edge of the film from an approximate analysis of Freund and Hu (1988) – see that reference for an accurate plot. Very near the edge the approximate solution breaks down.

2.3 Stresses in a Multilayer: Layer by Layer Deposition and Release from the Substrate

As depicted in Fig. 2.4, a multilayer with N layers is deposited layer by layer on a thick substrate. The intrinsic stress and deposition temperature for the i'th layer are σ_i^I and T_0^i, and the properties are designated by the subscript i. Assuming the substrate is very thick (and stiff) compared to the multilayer, the stress in each layer at temperature T will be given by (2.6), i.e.

$$\sigma_i^R = -\frac{E_i(\alpha_i - \alpha_s)}{(1 - \nu_i)}(T - T_0^i) + \sigma_i^I \tag{2.8}$$

where $\sigma_{11} = \sigma_{22} = \sigma_i^R$.

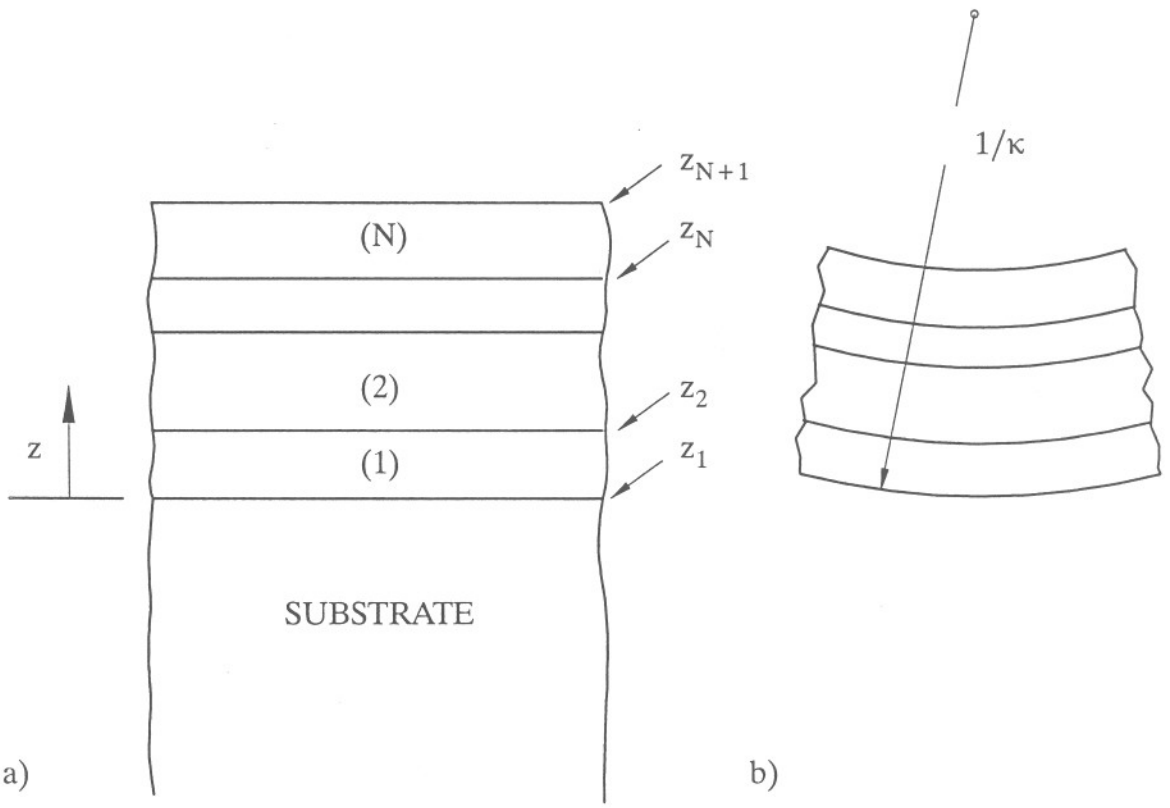

Fig. 2.4. Multilayer deposition. (a) Layer by layer deposition on a very thick substrate. (b) Release of the multilayer from the substrate at temperature T.

The multilayer is released from the substrate at temperature T. The inplane strain change relative to the attached state at T is

$$\Delta\epsilon_{11} = \Delta\epsilon_{22} \equiv \Delta\epsilon = \Delta\epsilon_0 - z\kappa \tag{2.9}$$

where $\Delta\epsilon_0$ is the value at the bottom at $z = 0$, and κ is the curvature change at release. The inplane *stress change* in the i'th layer is

$$\Delta\sigma_{11} = \sigma_{22} \equiv \Delta\sigma = \frac{E_i}{1-\nu_i}(\Delta\epsilon_0 - z\kappa) \tag{2.10}$$

The total stress in the i'th layer after release is $(\sigma_{11} = \sigma_{22} = \sigma)$

$$\sigma = \sigma_i^R + \Delta\sigma = \frac{E_i}{1-\nu_i}(\Delta\epsilon_0 - z\kappa) + \sigma_i^R \tag{2.11}$$

The equations for determining $\Delta\epsilon_0$ and κ are

$$\int_0^{z_{N+1}} \sigma dz = 0 \quad \text{and} \quad \int_0^{z_{N+1}} \sigma z dz = 0 \tag{2.12a,b}$$

These can be written as

$$\begin{aligned} C_{11}\Delta\epsilon_0 - C_{12}\kappa &= A_1 \\ C_{12}\Delta\epsilon_0 - C_{22}\kappa &= A_2 \end{aligned} \tag{2.13}$$

where

$$C_{11} = \sum_{i=1}^{N} \frac{E_i t_i}{(1-\nu_i)}\ ,\ C_{12} = \sum_{i=1}^{N} \frac{E_i(z_{i+1}^2 - z_i^2)}{2(1-\nu_i)}\ ,\ C_{22} = \sum_{i=1}^{N} \frac{E_i(z_{i+1}^3 - z_i^3)}{3(1-\nu_i)}$$

$$A_1 = -\sum_{i=1}^{N} t_i\sigma_i^R\ ,\ A_2 = -\sum_{i=1}^{N} \frac{1}{2}(z_{i+1}^2 - z_i^2)\sigma_i^R$$

Once $\Delta\epsilon_0$ and κ are obtained, σ can be evaluated from (2.11). The stress at the top of the i'th layer is given by (2.11) with $z = z_{i+1}$ and at the bottom with $z = z_i$. The average stress $\bar{\sigma}$ in the i'th layer is

$$\bar{\sigma} = \frac{E_i}{1-\nu_i}\left[\Delta\epsilon_0 - \frac{1}{2}(z_i + z_{i+1})\kappa\right] + \sigma_i^R \tag{2.14}$$

These results hold for the released multilayer at *any temperature* T, not only the release temperature. This follows from the fact that the deformation is elastic. The state at T does not depend on the temperature at which release occurs. This statement would not be true if plastic deformation occurred in any of the layers.

2.4 An Example: A Bilayer

We consider an example (taken from Evans and Hutchinson (1995)) of a bilayer by specializing the above results for $N = 2$. Suppose both layers are deposited at T_0 and that the intrinsic stresses are zero $\sigma_i^I = 0$, $i = 1,2$. We seek the stresses at temperature T. Recall that the stress will be independent of the release temperature. The problem is completely equivalent to one in which the two flat layers are bonded together at T_0.

The equations in Section 2.3 can be reduced with algebraic manipulation to the following equations for the stress σ at the top of layer 2 and the average stress $\bar{\sigma}$ in layer 2. With

$$\xi = \frac{h_2}{h_1}\ ,\ \Sigma = \frac{E_2/(1-\nu_2)}{E_1/(1-\nu_1)}\ ,\ \sigma^T = \frac{E_2}{1-\nu_2}(\alpha_1 - \alpha_2)(T - T_0) \tag{2.15}$$

$$\frac{\bar{\sigma}}{\sigma^T} = \frac{1 + \Sigma\xi^3}{(\Sigma\xi^2 - 1)^2 + 4\Sigma\xi(\xi + 1)^2} \tag{2.16}$$

$$\frac{\sigma}{\sigma^T} = \frac{1-3\Sigma\xi^2-2\Sigma\xi^3}{(\Sigma\xi^2-1)^2 + 4\Sigma\xi(\xi + 1)^2} \tag{2.17}$$

The curvature of the bilayer is

$$\kappa = \frac{6\xi^2(1+\xi)}{(\Sigma\xi^2-1)^2 + 4\Sigma\xi(\xi+1)^2}\left[\frac{(1-\nu_1)\sigma^T}{E_1 h_2}\right] \tag{2.18}$$

Plots of σ/σ^T and $\bar{\sigma}/\sigma^T$ for the entire range of relative layer thicknesses are given in Fig. 2.5.

The *misfit stress* σ^T defined in (2.15) is the stress in the upper layer which would occur if the lower layer were infinitely thick $(\xi = h_2/h_1 \to 0)$, as can be seen from (2.6). The above results indicate that the *average* residual stress is essentially the misfit stress, σ^T, when the film is *thin* $(\xi << 1)$, but is reduced to a fraction of σ^T when the film and substrate have comparable thicknesses, as plotted in Fig. 2.5 for three values of Σ. Bending has its maximum effect when the two layers have about equal thickness, resulting in substantial redistribution of the misfit stress. Specifically, and most importantly, the stress at the top of layer #2 develops the *opposite sign* from the misfit stress and becomes substantially larger in magnitude than the average stress in that layer, $\bar{\sigma}$, as seen in Fig. 2.5. The key features brought out in Fig. 2.5 are summarized as follows: (a) When layer 2 is sufficiently thin, $(\xi << 1)$, the residual stress in this layer is everywhere approximately the misfit stress σ^T. (b) Conversely, when layer 1 is relatively thin, $(\xi \to \infty)$, the stress throughout layer 2 approaches

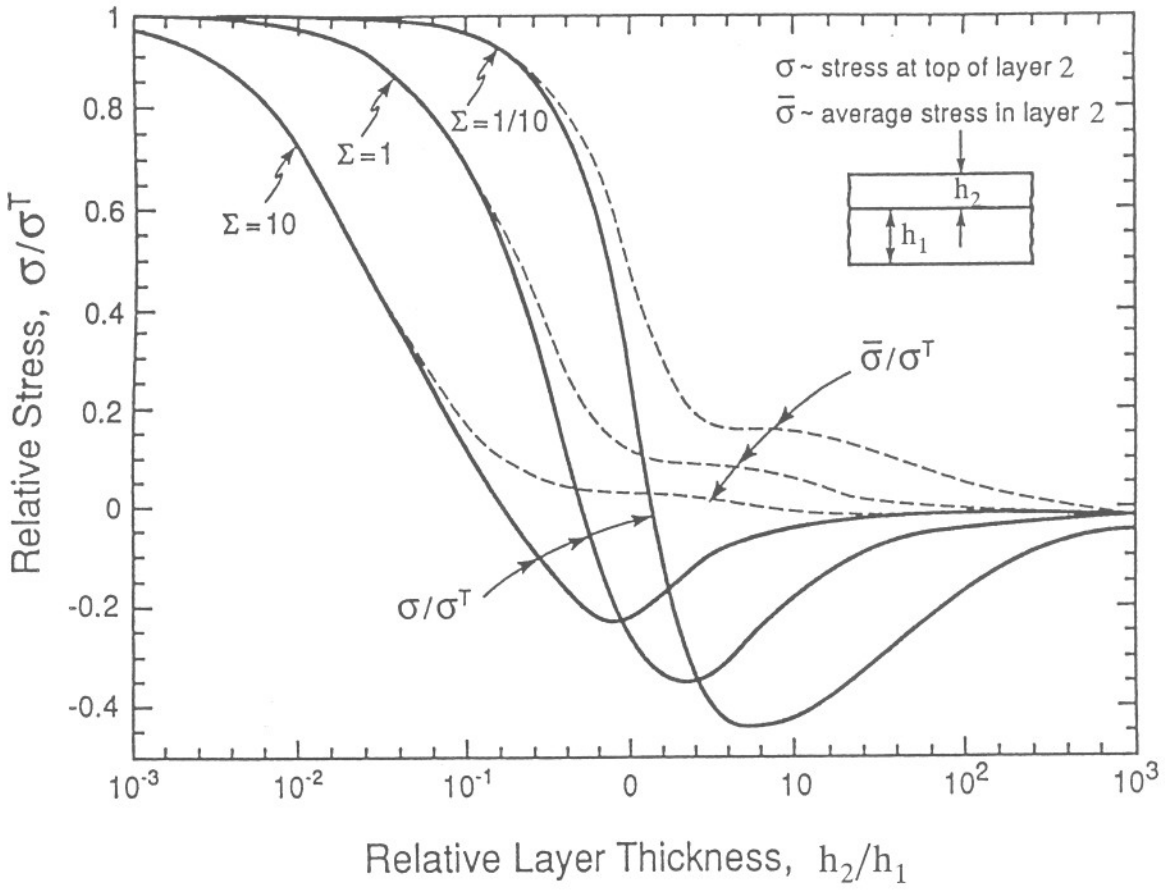

Fig. 2.5. Stress at the top surface, σ, and average stress in the top layer, $\bar{\sigma}$, of a bilayer.

zero. (c) Yet, in the intervening range of ξ, the stress σ at the top surface of layer 2 can have the opposite sign to σ^T and can be large compared to $\bar{\sigma}$. In particular, tensile stresses can arise at the surface of a film that would be in compression in the absence of bending. The range of ξ corresponding to such tensile stresses is of direct relevance to the crazing mode of film cracking. From Eqn. (2.11) it is seen that a tensile stress will exist at the top surface for all thickness ratios ξ greater than that satisfying $3\Sigma\xi^2 + 2\Sigma\xi^3 = 1$. For small Σ, the *minimum* ξ corresponds to $\xi \cong (1/2\Sigma)^{1/3}$; for $\Sigma = 1, \xi = 1/2$; while for large Σ, $\xi \cong (1/3\Sigma)^{1/2}$.

When the film (layer 2) is thin compared to the substrate (layer 1), the curvature κ is directly related to the stress in the film and is commonly used as a means of measuring film stress. To see this eliminate σ^T from (2.16) and (2.18) to obtain the following relation between κ and the average stress in the upper layer:

$$\kappa = \frac{1 + \xi}{1 + \Sigma\xi^3} \frac{6(1 - \nu_1)h_2\bar{\sigma}}{E_1 h_1^2} \tag{2.19}$$

For $\xi << 1$ and $\Sigma\xi^3 << 1$, one obtains the well known relation

$$\kappa = \frac{6(1 - \nu_1)h_2\bar{\sigma}}{E_1 h_1^2} \tag{2.20}$$

Note that the properties of the substrate on which the bilayer is deposited have no influence on the stresses or curvature of the released bilayer in this example, as should be expected in physical grounds. In general, however, α_s does effect the stresses and curvature of a released bilayer (or multilayer) when the deposition temperature differs from layer to layer.

2.5 Stresses in a Multilayer due to Through−Thickness Temperature Gradients

The results in Sections 2.2 and 2.3 were restricted to multilayers subject to uniform temperature. The analysis can be extended to account for a temperature difference between the top and bottom surfaces. When the temperature distribution has reached steady−state (i.e. independent of time), the temperature varies linearly in each layer. The steady−state temperature distribution is readily obtained. An analysis similar to that in Section 2.2 provides the stresses in each layer and the curvature of the multilayer.

3. SELECTED RESULTS FROM ELASTIC FRACTURE MECHANICS

The topics in this Section are selected from elastic crack mechanics because of their relevance to cracking of films and layers and their interfaces. Most of the topics are covered in more detail, including references, in the review article by Hutchinson and Suo (1992). The organization into subsections is

(3.1) Cracks in homogeneous solids – stress intensity factors, energy release rate and toughness.

(3.2) Interface cracks and interface toughness. Mixed mode effects.

(3.3) Crack kinking out of an interface.

(3.4) Crack deflection by an interface.

3.1 Cracks in Homogeneous Solids – Stress Intensity Factors, Energy Release Rate and Toughness

We consider linear isotropic solids with Young's modulus E and Poisson's ratio ν. Results from crack mechanics for 2D, plane strain elasticity will be cited.

Consider the generic body in Fig. 3.1. Take the origin of the (x_1, x_2)–axes at the crack tip and align the x_1–axis such that it is parallel to the crack. (If the crack is curved, x_1 is aligned with the tangent to the crack at the tip). Let (r, θ) be the associated planar polar coordinates. The body is loaded in the plane. For any loading, the crack tip fields as the crack tip approached (for either plane strain or plane stress) have the universal form (as $r \to 0$)

$$\sigma_{ij} = \frac{K_I}{\sqrt{2\pi r}} \tilde{\sigma}^{I}_{ij}(\theta) + \frac{K_{II}}{\sqrt{2\pi r}} \tilde{\sigma}^{II}_{ij}(\theta) \tag{3.1}$$

where K_I and K_{II} are the mode I and II *stress intensity factors*. The mode I field is symmetric about the crack line, while the mode II field is anti–symmetric. The intensity factors are normalized such that on the line ahead of the tip $(\theta = 0)$

$$\sigma_{22} = \frac{K_I}{\sqrt{2\pi r}} \quad , \quad \sigma_{12} = \frac{K_{II}}{\sqrt{2\pi r}} \tag{3.2}$$

where $\tilde{\sigma}^{I}_{12}(0) = 0$ and $\tilde{\sigma}^{II}_{22}(0) = 0$.

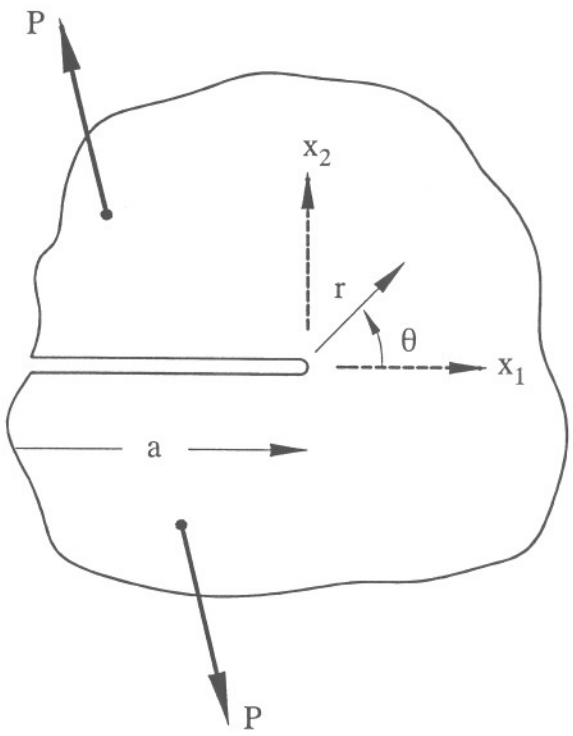

Fig. 3.1. Generic plane strain crack problem.

A crack problem is said to be a mode I problem if $K_{II} = 0$ and vise versa. Any problem where the geometry and loading is symmetric with respect to a straight crack is necessarily mode I. If the geometry is symmetric and the loading is anti−symmetric, the problem is mode II. (Out−of−plane loads induce shear tractions, σ_{13}, on the plane ahead of the tip. These are called mode III problems). Stress intensity factors have dimension stress × length$^{1/2}$. Comprehensive compilations of results for stress intensity factors are given by Tada, Paris and Irwin (1985) and Murakami (1987). Two results which will be used later in these notes are those for the two problems shown in Fig. 3.2. The classical problem for a straight crack of length 2a in an infinite body subject to remote stress σ_{ij}^{∞} has

$$K_I = \sigma_{22}^{\infty}\sqrt{\pi a} \quad , \quad K_{II} = \sigma_{12}^{\infty}\sqrt{\pi a} \quad , \quad K_{III} = \sigma_{23}^{\infty}\sqrt{\pi a} \tag{3.3}$$

The problem of an edge crack of length a in a semi−infinite half−space subject to remote stress σ_{22}^{∞} parallel to the free surface has

$$K_I = 1.1215\,\sigma_{22}^{\infty}\sqrt{\pi a} \tag{3.4}$$

Elasticity theory provides the elastic energy released by the solid to the crack tip under crack advance. In elastic fracture mechanics, this is the energy available to the fracture process. In what follows we state Irwin's relation between the *energy release rate*, G, and the stress intensity factors. (Derivations are given in most texts on fracture mechanics).

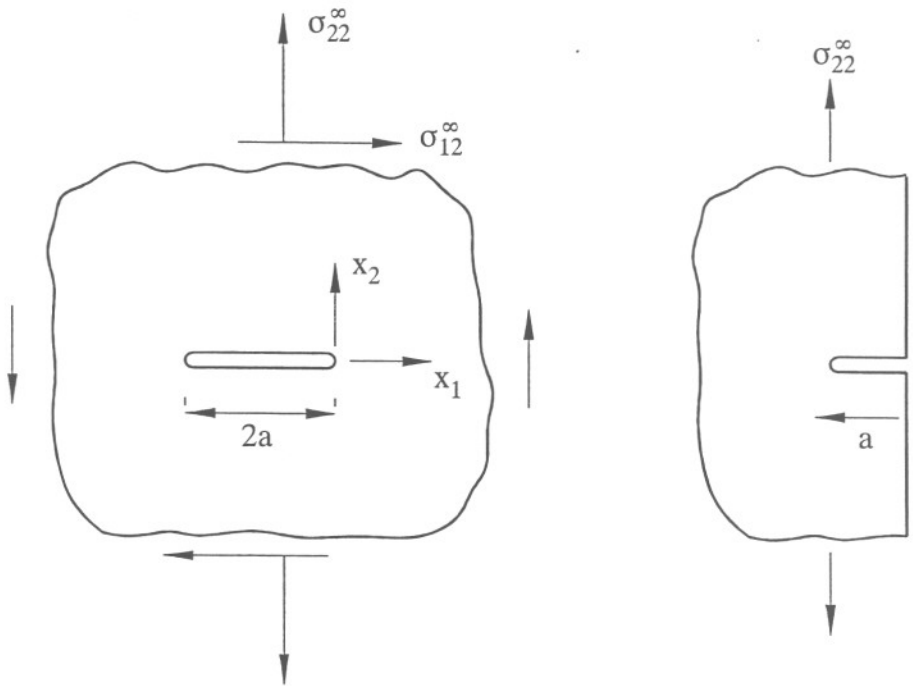

Fig. 3.2. Two crack problems.

The result given below is limited to crack advance *straight ahead* of the current crack direction. Crack kinking is excluded – it will be discussed later. Let PE(a) be the potential energy per unit thickness in the x_3–direction for an elastic body loaded either under *prescribed load* or *prescribed displacement*. Define the energy release rate to be the energy lost by the system (per unit thickness) due to crack advance:

$$G = -\frac{dPE}{da} \tag{3.5}$$

In a given state, G is independent of whether the load is prescribed or displacement is prescribed or any combination thereof. The Irwin connection for plane strain is

$$G = \frac{1-\nu^2}{E}\left(K_I^2 + K_{II}^2\right) \tag{3.6}$$

(The lead coefficient is 1/E for plane stress). G has dimensions of surface energy, energy per unit area, which is usually quoted in units Jm^{-2} in fracture mechanics.

For homogeneous solids, the *fracture toughness* is defined as the critical value of K_I or G as determined by a test of a mode I specimen. The details required for a valid mode I fracture toughness test are described in fracture mechanics texts. In particular, for elastic results such as (3.3) and (3.6) to apply any plasticity must be confined to a small region at the crack tip – conditions referred to as *small scale yielding*. The critical value of K_I measured in a valid mode I test is denoted by K_{Ic} and is called the fracture toughness. Equiva-

lently, by (3.6), one can use the critical value of G as the toughness. Here the critical G will be denoted by Γ_c (units Jm^{-2}) . For mode I, the two toughness measures are related by

$$\Gamma_c = \frac{1 - \nu^2}{E} K_{Ic}^2 \tag{3.7}$$

3.2 Interface Cracks and Interface Toughness. Mixed Mode Effects

As shown in Fig. 3.3, a crack lies on the interface between two dissimilar, but isotropic, elastic solids. Plane strain is again assumed. Because of the dissimilarity in elastic properties, there will usually be some asymmetry near the crack tip even if the geometry and loading are symmetric. By their nature (and because of the loadings), interface cracks tend to be *mixed mode*. Universal crack tip fields exist for the bimaterial interface crack with two stress intensity factors, but the fields are somewhat more complicated than those for the homogeneous solid. Details are discussed in Section II.C of Hutchinson and Suo (1992). Here, attention will be limited to a sub−class of elastic mismatches for which the near tip stress fields are identical to those for the homogeneous solid. Little is lost by restricting consideration in this way.

For the general bimaterial interface problem in plane strain, two elastic mismatch parameters – the Dundurs mismatch parameters – play a role in any traction boundary value problem:

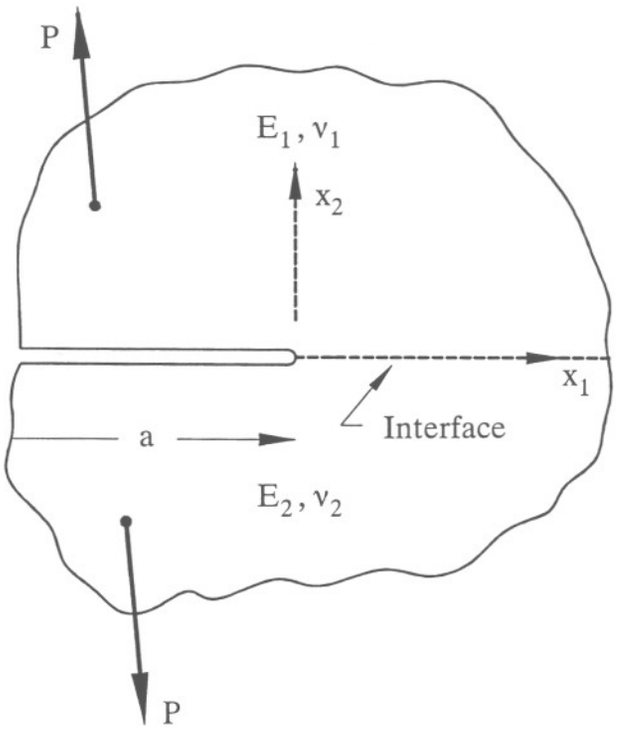

Fig. 3.3. An interface crack for a bimaterial.

$$\alpha_D = \frac{\overline{E}_1 - \overline{E}_2}{\overline{E}_1 + \overline{E}_2} \quad , \quad \beta_D = \frac{1}{2}\frac{\mu_1(1 - 2\nu_2) - \mu_2(1 - 2\nu_1)}{\mu_1(1 - \nu_2) + \mu_2(1 - \nu_1)} \tag{3.8}$$

where $\overline{E} = E/(1 - \nu^2)$ is the plane strain tensile modulus and $\mu = E/[2(1 + \nu)]$ is the shear modulus. The complications in the crack tip fields referred to above arise when β_D is non−zero. When $\beta_D = 0$, the stresses at the crack tip are the same as for the homogeneous solid (3.1), and, in particular, (3.2) apply such that K_I controls the normal stress acting on the interface ahead of the tip and K_{II} controls the shear stress. Discussion of the role of β_D and the justification for ignoring this role (by taking $\beta_D = 0$) is given in Section II.C of the reference cited. The first mismatch parameter α_D does play an important role in some problems. In some cases below, the role of β_D will also be displayed.

The relation between the energy release rate and stress intensity factors for crack advance *in the interface* is

$$G = \frac{1 - \beta_D^2}{2}\left[\frac{1 - \nu_1^2}{E_1} + \frac{1 - \nu_2^2}{E_2}\right](K_I^2 + K_{II}^2) \tag{3.9}$$

generalizing (3.6). This is the expression for arbitrary β_D. It can be seen that the second Dundurs parameter plays a very minor role in this connection, since β_D^2 is usually much smaller than 0.1.

Given the mixed mode nature of most interface crack problems, both K_I and K_{II} are needed to characterize the stresses on the interface. Equivalently, one can use G and the following measure of the relative proportion of mode II to mode I

$$\psi = \tan^{-1}(K_{II}/K_I) \tag{3.10}$$

Thus, $\psi = 0^o$ corresponds to pure mode I and $\psi = \pm 90^o$ to pure mode II. The pair (G, ψ) is now commonly used to characterize the intensity of an interface crack. Two crack problems are shown in Fig. 3.4. For the crack of length $2a$ on interface of an infinite bimaterial, elastic mismatch has no influence on the crack tip intensities when $\beta_D = 0$. Thus, (3.3) still holds and

$$G = \frac{1}{2}\left[\frac{1 - \nu_1^2}{E_1} + \frac{1 - \nu_2^2}{E_2}\right]\pi a\left(\sigma_{22}^{\infty\,2} + \sigma_{12}^{\infty\,2}\right) \quad , \quad \psi = \tan^{-1}\left(\frac{\sigma_{12}^{\infty}}{\sigma_{22}^{\infty}}\right) \tag{3.11}$$

For the thin film subject to uniform residual tension σ in the bonded state

$$G = \frac{1}{2}\frac{(1 - \nu_1^2)\sigma^2 h}{E_1} \quad , \quad \psi = \omega(\alpha_D) \tag{3.12}$$

where ω is sketched in Fig. 3.4. The result is valid once the crack length exceeds several film thicknesses where steady–state has set in and G is independent of crack length. Note that G is independent of α_D but ψ has some dependence. Note also that the interface experiences roughly equally levels of normal and shear stress in this case. The method for obtaining this solution will be discussed later in the notes. It and solutions for other interface crack problems are given in the article by Hutchinson and Suo (1992).

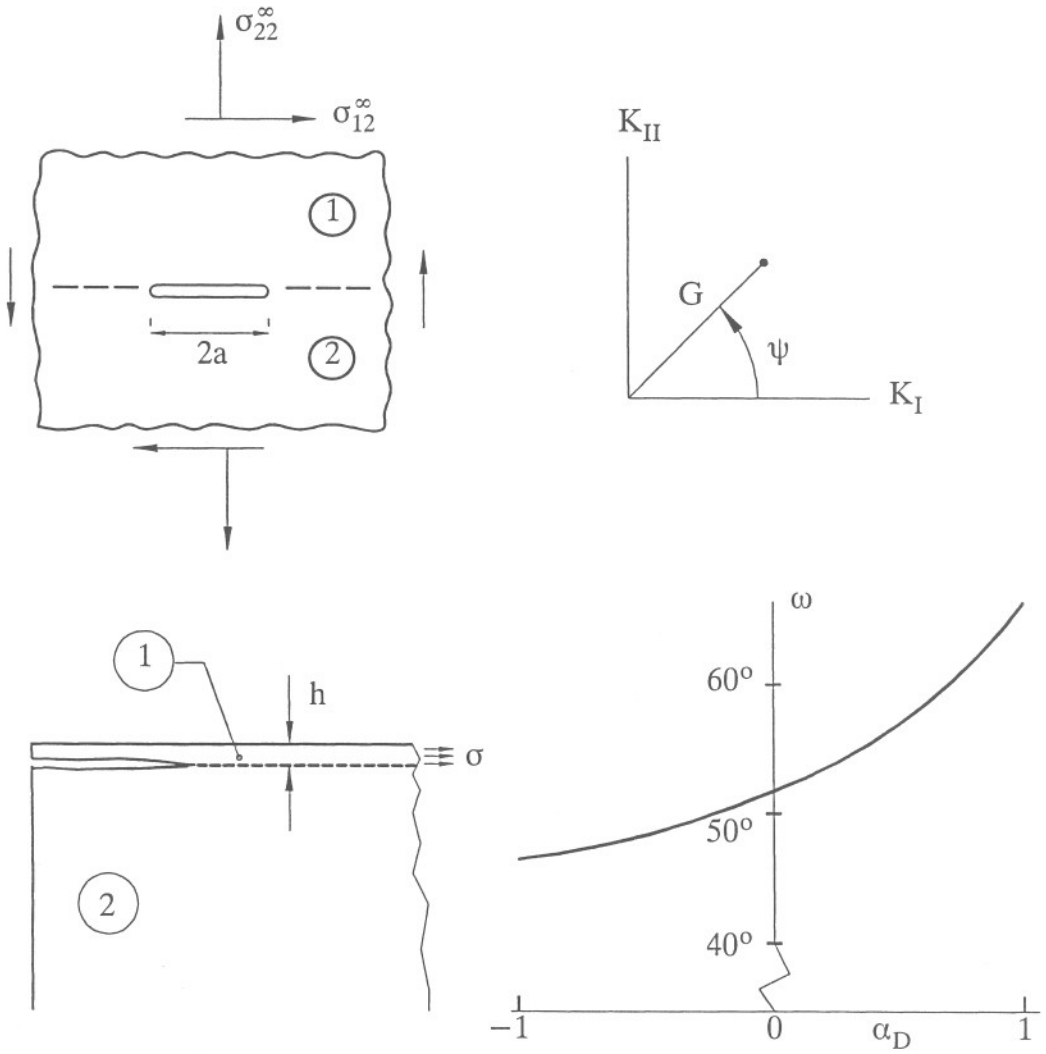

Fig. 3.4. Two interface crack problems: an interface crack for a remotely stressed bimaterial and an interface crack between a thin film and substrate.

Interface toughness is defined as the critical value of G needed to advance the crack, assuming it propagates in the interface. It is again denoted by Γ_c. It has been found that the interface toughness depends strongly on the mode mixity ψ for the interfaces for which experimental data exists. This is emphasized by writing the interface toughness as $\Gamma_c(\psi)$. Data from Liechti and Chai (1992) for an epoxy/glass interface is presented in Fig. 3.5. The lowest toughness for thus interface, and others for which data is available, is the mode I toughness. In this case, the near mode II toughness is nearly ten times larger. The toughness values presented in Fig. 3.5 correspond to "steady–state" toughness for which initial resistance

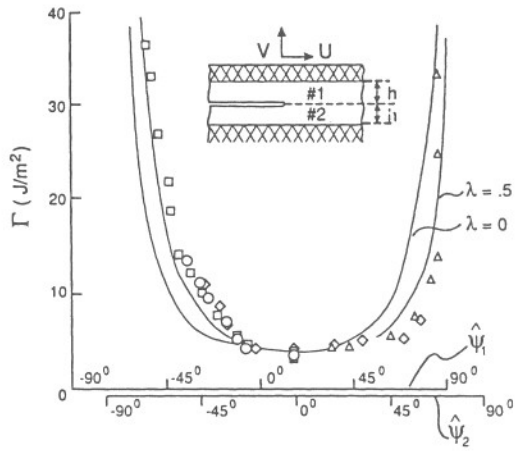

Fig. 3.5. Toughness $\Gamma_c(\psi)$ of a glass/epoxy interface as dependent on the mode mixity ψ. Data from Liechti and Chai (1992).

to growth (G increasing with a) is overcome and the crack propagates at essentially constant G. The two $\psi-$measures in Fig. 3.5 are related to the role of β_D for this system. The elastic mismatch is large and $\beta_D \cong .2$. This affects the definition of ψ, as discussed in the article by Hutchinson and Suo (1992).

3.3 Crack Kinking Out of an Interface

Will a loaded interface crack propagate in the interface or will it kink out of the interface and propagate into either of the adjoining materials? The answer depends on the energy release rates for interface advance versus kinking, and on the relative toughnesses of the interface and the adjoining materials.

We begin with the mechanics of interface kinking first. An interface crack is loaded to (G, ψ). Consider a putative kink crack (Fig. 3.6) of length a. Denote the intensity of the kink crack tip by $\left(G_{tip}, \psi_{tip}\right)$. In the limit where a is very small compared to the parent interface crack,

$$\frac{G_{tip}}{G} = f_1(\Omega, \psi, \alpha_D) \quad \text{and} \quad \psi_{tip} = f_2(\Omega, \psi, \alpha_D) \tag{3.13}$$

where Ω is the kink crack angle and it is again assumed that $\beta_D = 0$. We take $\psi > 0$ and anticipate that the crack will kink into the lower material (#2). (The results which follow permit the roles of #1 and #2 to be switched when $\psi < 0$). The solution to the elasticity problem for the putative kink crack provides f_1 and f_2 in (3.13). In the plot in Fig. 3.6, $(G_{tip})_{max}$ denotes the maximum value of G_{tip} over all Ω for a given (G, ψ). Except for $\alpha_D < -2/3$, the angle Ω which maximizes G_{tip} also gives $\psi_{tip} \cong 0$. In other words, to a reasonably good approximation, the kink angle which maximizes the energy release rate of the kink crack corresponds to mode I. (Kink angles are presented by He and Hutchinson (1989)).

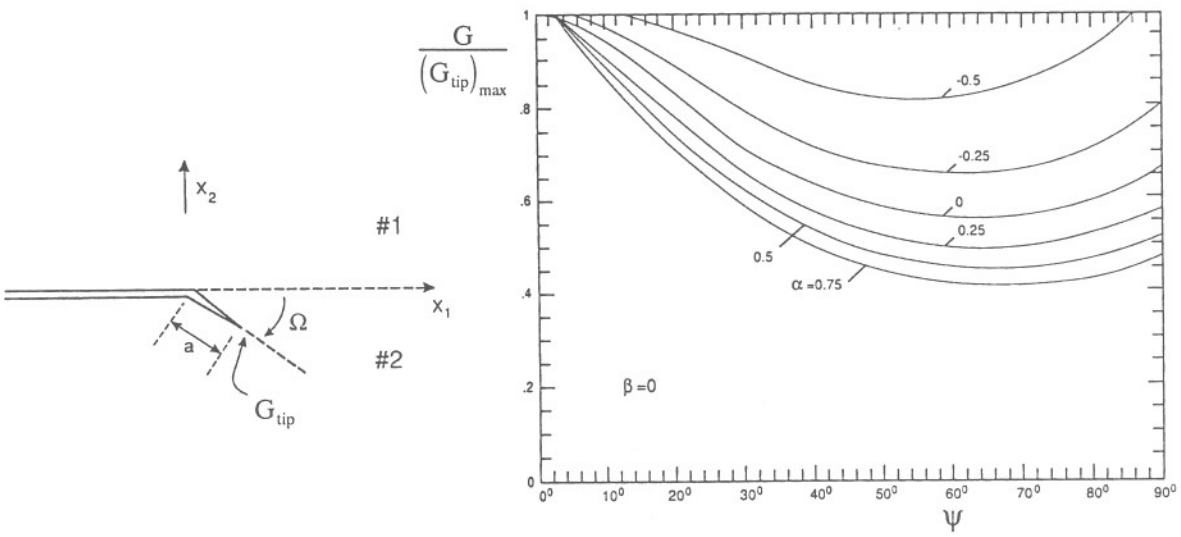

Fig. 3.6. Crack kinking out of an interface. Rates of energy release rate for advance in the interface to the maximum energy release rate for the kinked crack as a function of mode mixity ψ for various elastic mismatches ($\beta_D = 0$).

The ratio $G/(G_{tip})_{max}$ in Fig. 3.6 is ratio of energy release rate for advance in the interface to that for kinking into material #2. The kinked crack's rate can be as much as twice that for propagation in the interface, depending on ψ and elastic mismatch. Whether the crack kinks or advances in the interface depends on the relative toughnesses. Let $\Gamma_c^{(2)}$ be the toughness of material #2, and let $\Gamma_c(\psi)$ be the toughness of the interface. Consider loading such that G increases monotonically with ψ fixed. If

$$\frac{G}{\left(G_{tip}\right)_{max}} < \frac{\Gamma_c(\psi)}{\Gamma_c^{(2)}} \tag{3.14}$$

the condition $(G_{tip})_{max} = \Gamma_c^{(2)}$ will be met prior to the condition $G = \Gamma_c(\psi)$, and the crack will kink. Conversely, of the inequality in (3.14) is switched the crack will advance in the interface. Graphically, if the point $\Gamma_c(\psi)/\Gamma_c^{(2)}$ is plotted in Fig. 3.6 and if it falls above the curve for the appropriate elastic mismatch, then kinking will occur. Otherwise, it will not.

3.4 Crack Deflection at an Interface

Consider the competition depicted in Fig. 3.7 between *penetration* of a crack through an interface and *crack deflection* into the interface (kinking into the interface). The parent crack has its tip at the interface and is aligned perpendicular to the interface. Stressing is taken to be symmetric with respect to the parent crack. Let $(G_{tip})_p$ denote the energy release rate of the penetrating crack, which by symmetry is a mode I crack. Let $(G_{tip})_d$ denote the energy release rate of the deflected interface crack and let ψ_{tip} denote its mode mixity.

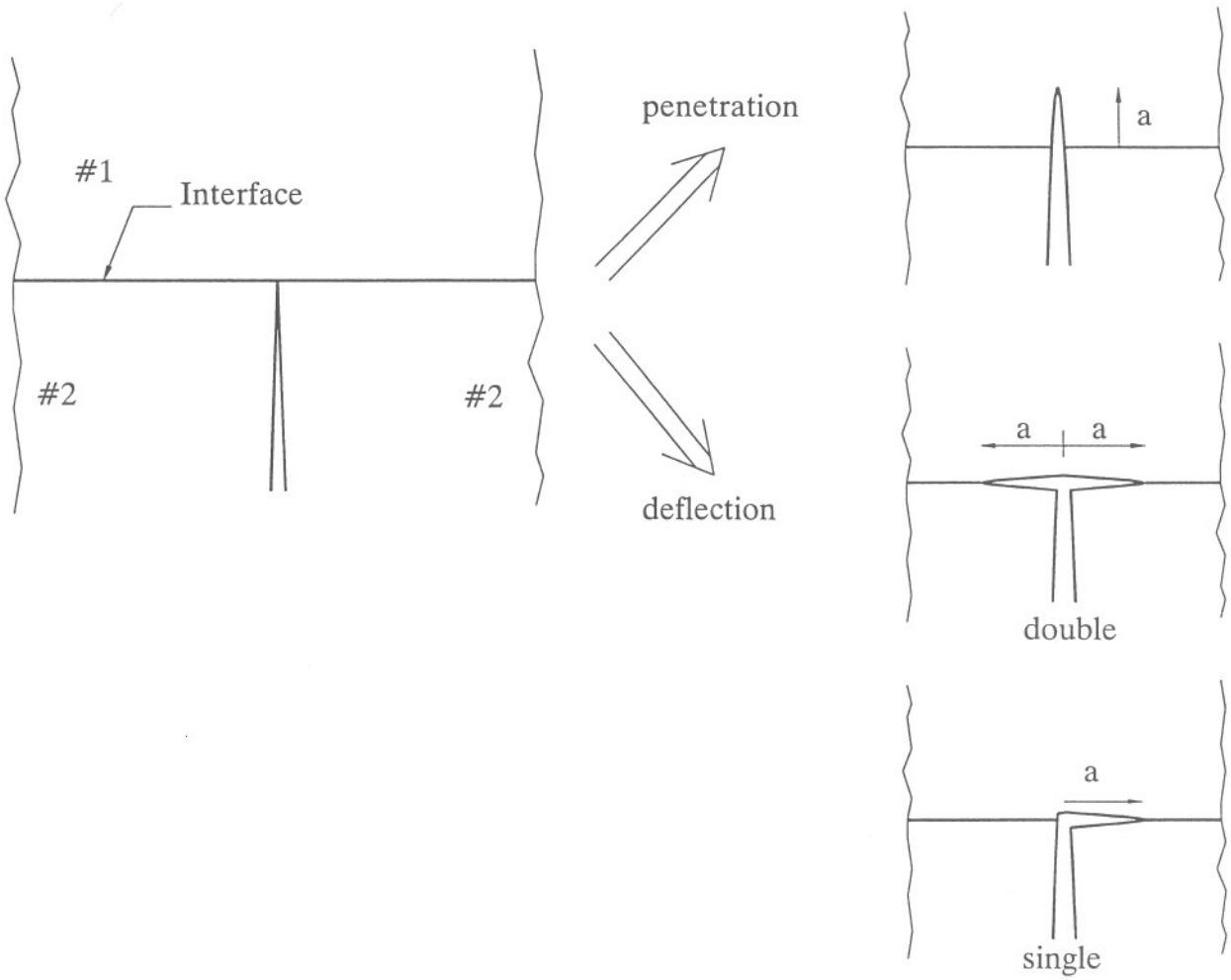

Fig. 3.7. Crack arrested at an interface under symmetric loading. Under increasing load, will the crack advance by penetrating the interface or by deflecting into the interface?

At *equal putative crack lengths*, a , the ratio of the energy release rates of the competing crack propagation modes depends only on α_D (with $\beta_D = 0$) (see He *et al.* (1994) for full details). Plots of this ratio are given in Fig. 3.8, along with the corresponding ψ_{tip} for the deflected interface crack. There is very little difference between the doubly–deflected crack and the singly–deflected crack.

The competition between deflection and penetration is settled by the ratio of the interface toughness to that of material #1. As in the argument made for kinking, if

$$\frac{\left(G_{tip}\right)_d}{\left(G_{tip}\right)_p} < \frac{\Gamma_c(\psi)}{\Gamma_c^{(1)}} \tag{3.15}$$

conditions for penetration will be attained prior to those for deflection, and vise versa. Note from Fig. 3.8, that except for large elastic mismatches, penetration is likely if the interface toughness exceeds about 1/4 of the toughness of the material across the interface.

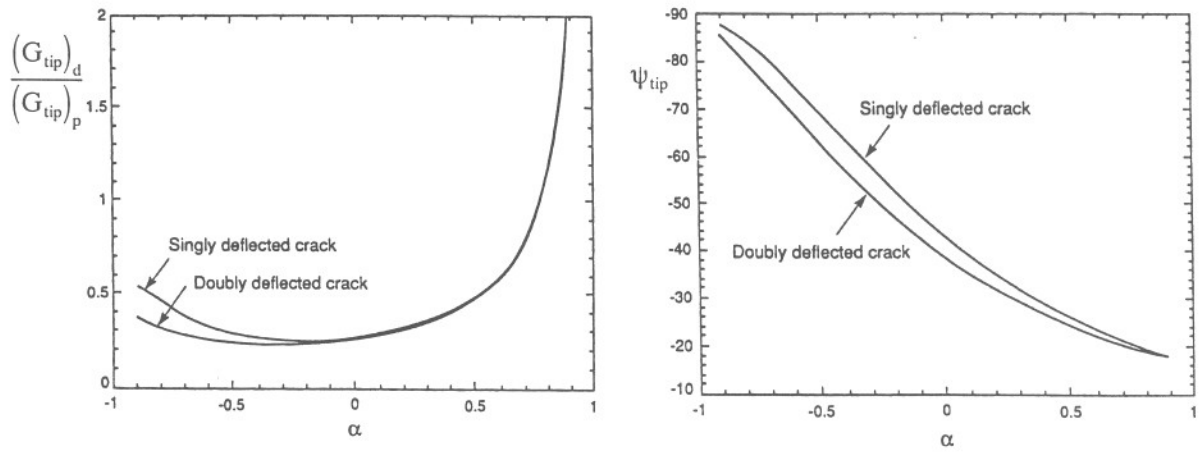

Fig. 3.8. Ratio of the energy release rate for crack deflection to that for penetration at equal putative crack lengths a . Mode mixity ψ_{tip} for the deflected interface crack for the tip on the right hand side.

4. THROUGH–CRACKS IN FILMS AND LAYERS

The principles underlying through–cracks in a embedded layer are similar to those for a film. The first sub–section focuses of films, the second on embedded layers. The concept of *steady–state crack propagation* is central to the mechanics of film and layer cracking, as well as interface cracking, and we address this issue next.

4.1 Single Cracks in Films under Tension

Consider the 3–D crack in Fig. 4.1 of length a advancing quasi–statically in the x_3–direction. A tensile residual stress σ exists in the film prior to cracking. The results derived below apply to either $\sigma_{11} = \sigma$ and $\sigma_{33} = 0$ or $\sigma_{11} = \sigma_{33} = \sigma$. The crack extends to the substrate interface. Symmetry dictates that the crack front advancing through the film experiences mode I conditions, with K_I varying along the front edge in a manner dependent on the shape of the front. With $G = (1 - \nu_1^2)K_I^2/E_1$, let $\overline{G}$ be the average of G through the thickness,

$$\overline{G} = \frac{1}{h}\int_0^h G\, dx_2 \tag{4.1}$$

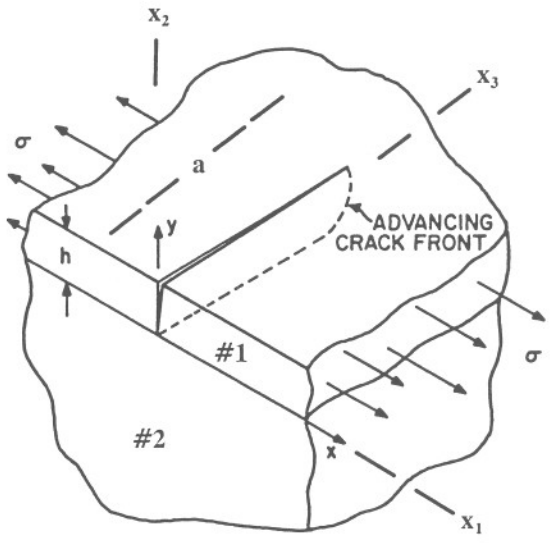

Fig. 4.1. A 3D through–crack channeling across a film.

A *qualitative* plot of $\overline{G}$ as a function of a/h is shown in Fig. 4.2. For cracks shorter than about one film thickness, the energy release rate falls well below the asymptote $\overline{G}_{ss}$. As the crack grows beyond about 2 film thicknesses, $\overline{G}$ increases monotonically and the crack front very quickly settles into *steady–state* conditions such that $\overline{G}$ becomes *independent* of crack length a. The advancing tip no longer "feels" any influence of the other end of the crack. The steady–state energy release rate is

$$\overline{G}_{ss} = \frac{\pi}{2}\frac{(1-\nu_1^2)}{E_1}\sigma^2 h\, g(\alpha_D, \beta_D) \tag{4.2}$$

where g will be presented below along with its derivation. Few fully 3D solutions for film or layer cracks exist which show the *quantitative* transition to steady state. One such solution is available for a crack interior to a film with an initial elliptical–type shape (Nakamura and Kumar). That solution displays a transition to steady–state in accord with the depiction in Fig. 4.2.

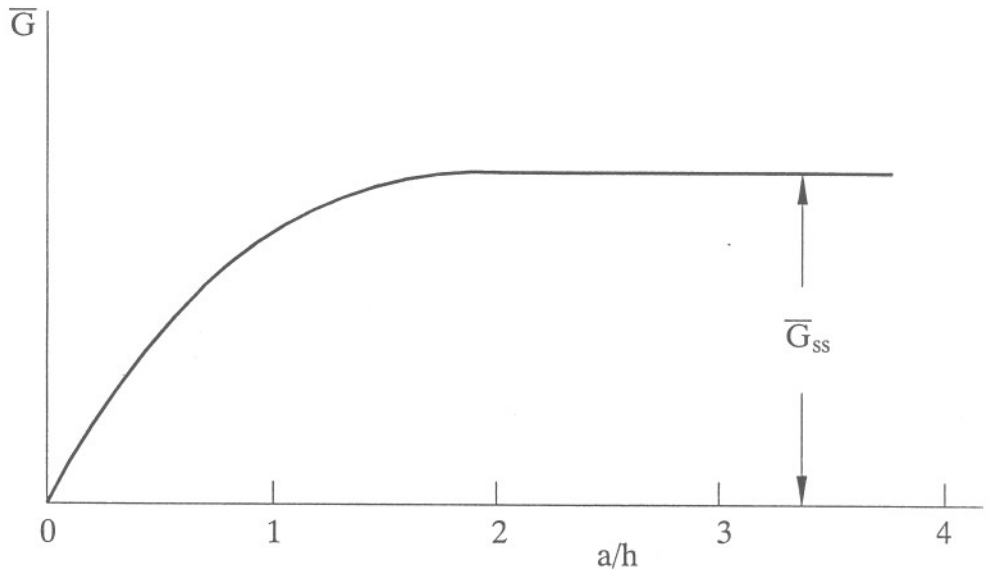

Fig. 4.2. Qualitative approach to steady–state channeling.

To analyse *steady–state channeling* we make use of Fig. 4.3 which depicts how $\overline{G}_{ss}$ can be determined from a 2D plane strain solution. In steady–state, the energy released for an advance da of the crack is $\overline{G}_{ss} h\, da$. This must be equal to the potential energy difference between slabs of thickness da upstream and downstream. Since the remote stress σ in the film does no work during cracking, this is the same as the strain energy difference between the slabs, i.e.

$$h\overline{G}_{ss} = \left[(SE)_{Upstream} - (SE)_{Downstream}\right] \tag{4.3}$$

where SE denotes the strain energy per unit thickness in the x_3–direction. Each of the two slabs is in a state of plane strain. By the cartoon in the lower half of Fig. 4.3, the strain energy difference in (4.3) is precisely the work done by tractions in the *reduced problem* such that

$$h\overline{G}_{ss} = h\int_0^{\overline{\delta}} \sigma(\overline{\delta})\, d\overline{\delta} = \frac{1}{2}\sigma\overline{\delta}h \tag{4.4}$$

where $\overline{\delta}$ is the average crack opening displacement.

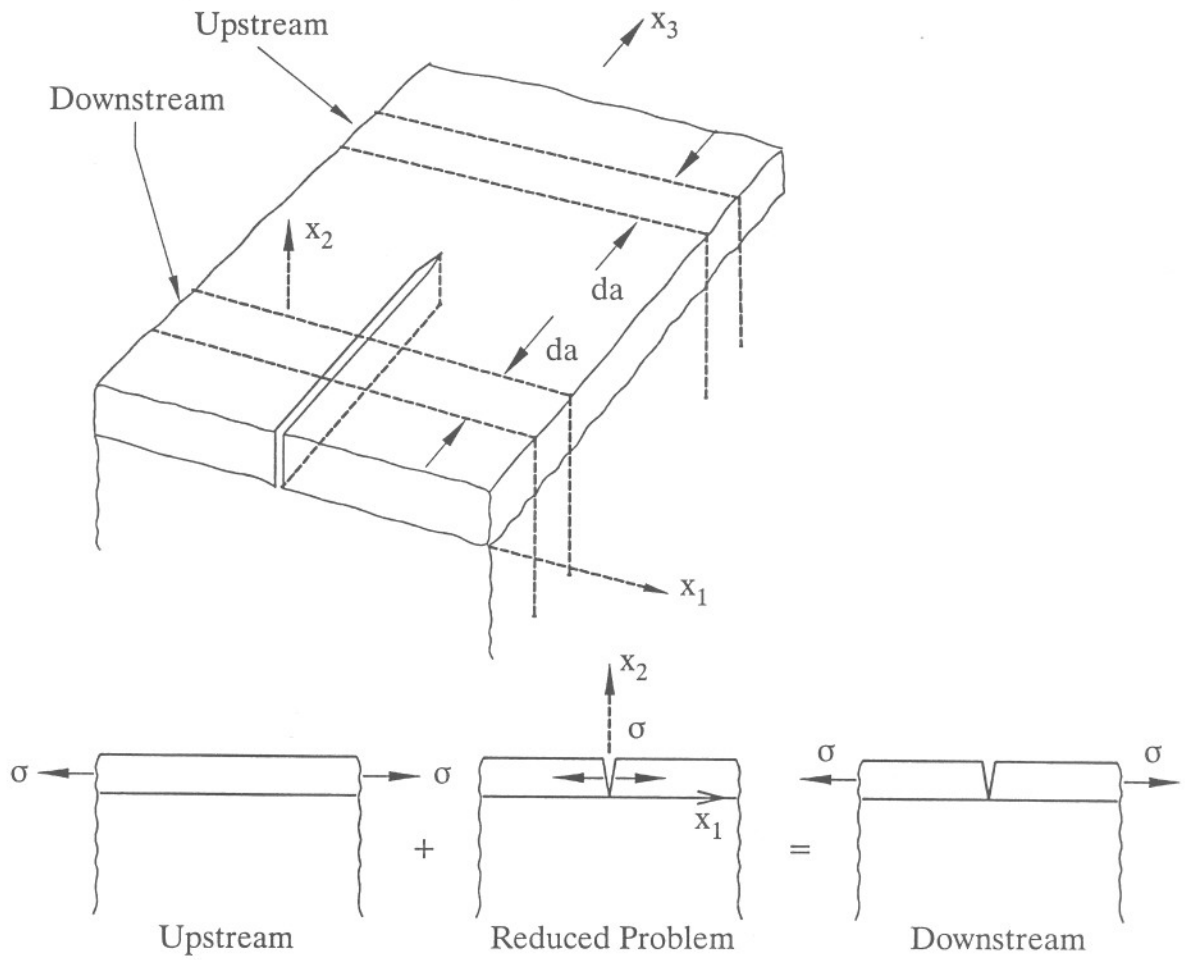

Fig. 4.3. Energy accounting in steady–state channeling. The energy release rate can be determined from the reduced problem – a plane strain problem.

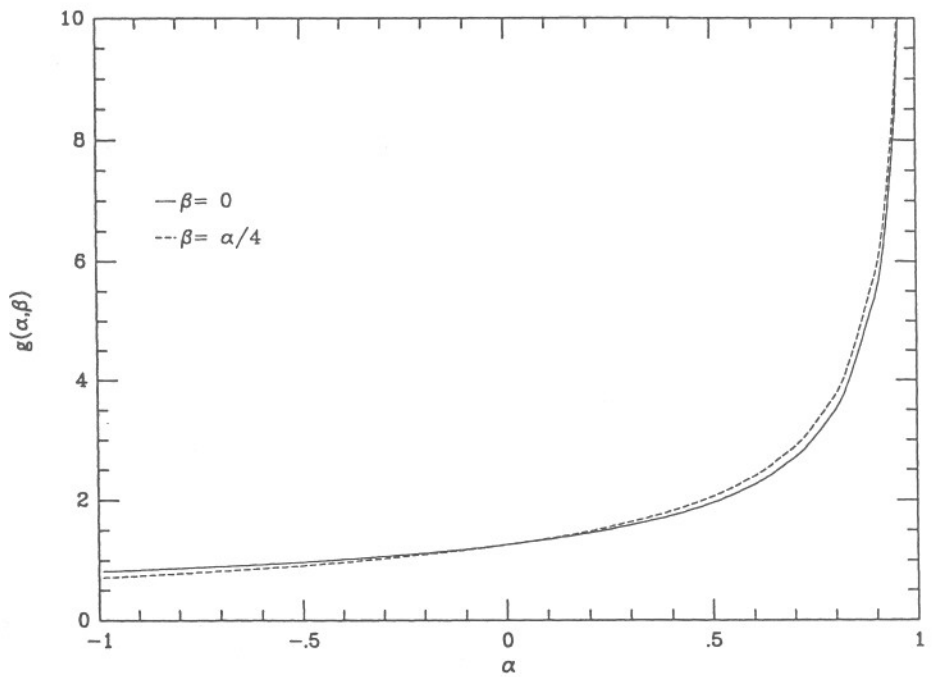

Fig. 4.4. Plot of $g(\alpha_D, \beta_D)$ in (4.2).

The reduced problem is a plane strain problem. By dimensional considerations and linearity, it follows that $\overline{\delta} = c(1 - \nu_1^2)\sigma h/E_1$ where c is a dimensionless function of α_D and β_D. The form (4.2) follows directly from (4.4). Computed values of g in (4.2) are plotted in Fig. 4.4 from Beuth (1992). The effect of elastic mismatch is substantial, especially when the film is stiff compared to the substrate $(\alpha_D > 0)$.

It is useful to record an alternative expression to (4.4) for $\overline{G}_{ss}$. Denote the energy release rate of a plane strain edge crack of depth b $(b \le h)$ in the reduced problem by $G_{ps}(b)$. The work done (4.4) by the tractions in the reduced problem is precisely the energy released by the edge crack in advancing from $b = 0$ to $b = h$ (since it is an elastic problem). Thus, one can also write

$$h\overline{G}_{ss} = \int_0^h G_{ps}(b)db \tag{4.5}$$

Noting the edge crack result (3.4) and (3.6), it can immediately be shown that for no elastic mismatch $(\alpha_D = \beta_D = 0)$

$$\overline{G}_{ss} = \frac{\pi}{2}(1.1215)^2 \frac{\left(1 - \nu_1^2\right)\sigma^2 h}{E_1} \tag{4.6}$$

The condition excluding steady–state channel cracking in a thin film is $\overline{G}_{ss} < \Gamma_c^{(1)}$, where $\Gamma_c^{(1)}$ is the mode I toughness of the film. By (4.2) this condition can be written in the form (1.1) introduced in the Overview, i.e.

$$\Omega < \Omega_c \ ; \ \text{where} \ \ \Omega = \frac{\left(1 - \nu_1^2\right)\sigma^2 h}{E_1 \Gamma_c^{(1)}} \ \text{and} \ \Omega_c = \frac{2}{\pi g(\alpha_D, \beta_D)} \tag{4.7}$$

Because the energy release rate approaches $\overline{G}_{ss}$ from below (c.f. Fig. 4.2), condition (4.7) ensures that no film cracks will propagate. In this sense it is a *fail safe criterion*. If the initial flaws in the film are all sufficiently small compared to h, (4.7) may be overly conservative.

With respect to the discussion of the possibility of crack penetration and deflection at an interface in Section 3.4, it is of interest to note that

$$\overline{G}_{ss} = \frac{1}{2} G_{ps}(h) \tag{4.8}$$

for the case of no elastic mismatch $(\alpha_D = \beta_D = 0)$. In this case, for channel cracking to occur unaccompanied by either interface cracking or substrate penetration, it is required that (c.f. Section 3.4)

$$\Gamma_c^{(2)} > 2\Gamma_c^{(1)} \text{ and } \Gamma_c(\psi) > \frac{1}{2}\Gamma_c^{(1)} \tag{4.9}$$

Another connection can be noted between (4.8) and steady–state film debonding (3.12) such that

$$\begin{aligned} \left(\overline{G}_{ss}\right)_{\text{cracking}} &= \pi g (G_{ss})_{\text{debonding}} \\ &= 3.95 (G_{ss})_{\text{debonding}} \text{ for } \alpha_D = \beta_D = 0 \end{aligned} \tag{4.10}$$

Steady–state debonding constitutes complete debonding of the film. Thus, assuming substrate penetration is excluded, the following modes of film failure exist depending on the interface to film toughness ratio (for $\alpha_D = \beta_D = 0$):

$$\frac{1}{2} < \Gamma_c(\psi)/\Gamma_c^{(1)} \Leftrightarrow \text{Cracking with no delamination}$$

$$.253 < \Gamma_c(\psi)/\Gamma_c^{(1)} < \frac{1}{2} \Leftrightarrow \text{Cracking with partial delamination}$$

$$\Gamma_c(\psi)/\Gamma_c^{(1)} < .253 \Leftrightarrow \text{delamination}$$

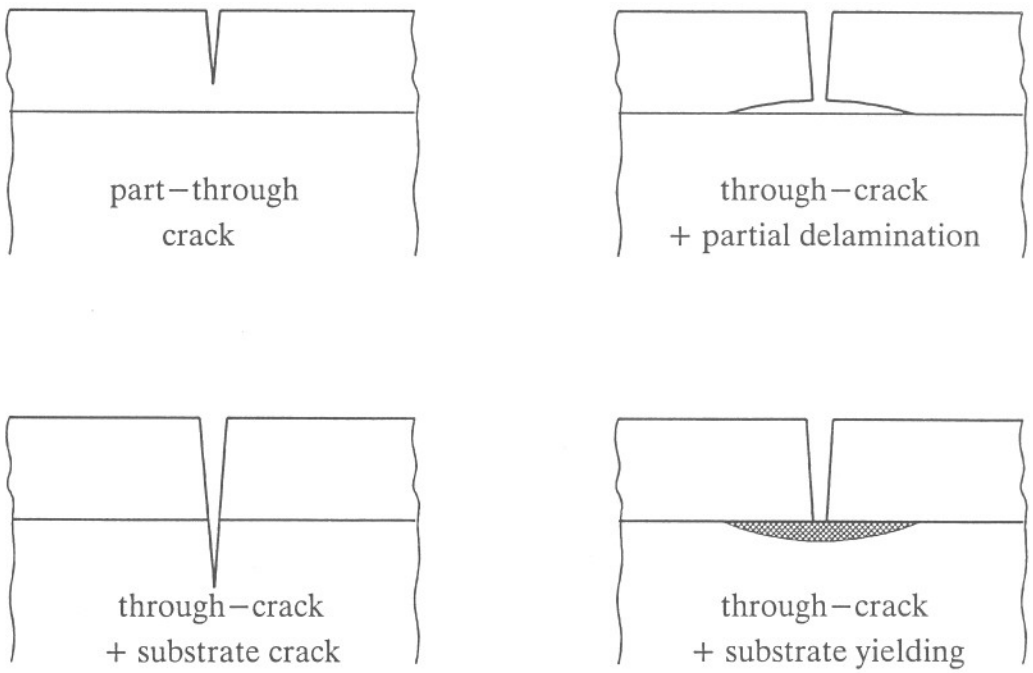

Fig. 4.5. Modes of film cracking.

These and other modes of film failure are shown in Fig. 4.5. Partial delamination, substrate cracking and substrate yielding each *increase* the energy release rate available for propagating the channeling film crack. Note that each results in a larger opening of the crack than would occur otherwise. A plane strain analysis is appropriate in each case, as illustrated in this Section. If the substrate is very stiff compared to the film, the crack may not extend all the way down to the interface (Beuth, 1992). The effect is usually small resulting in little change from the prediction for the through−crack. Results for the effect of substrate cracking accompanying film crack are given in the article by Hutchinson and Suo (1992). Recent work on the effect of substrate yielding has been given by Beuth and Klingbeil (1996).

4.2 Tunnel Cracks in Layers

The concept discussed in connection with film cracks apply as well to tunneling cracks in layers. In steady state tunneling

$$\overline{G}_{ss} = \frac{\left(1 - \nu_2^2\right)}{E_2}\sigma^2 h F \tag{4.11}$$

where σ is the stress in the layer, h is its thickness, ν_2 and E_2 its Poisson's ratio and Young's modulus, and F is a dimensionless function of the moduli ratios and thickness ratios of the other layers. As in the film problem F can be obtained from a plane strain analysis with (4.4) and (4.5) still applicable.

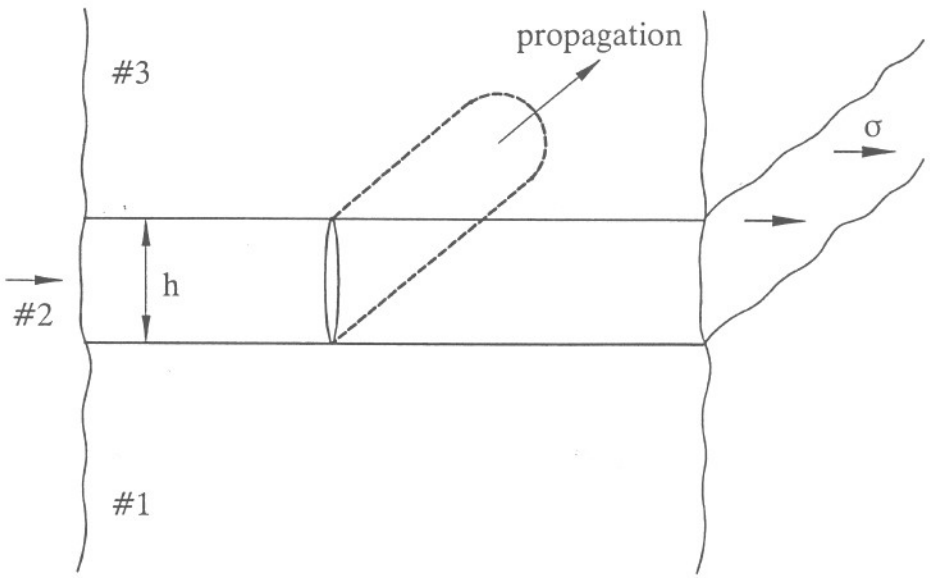

Fig. 4.6. Tunnel cracking in a layer under tensile stress.

Consider first the case of a layer sandwiched between two semi−finite layers (Fig. 4.6) where all three layers have the same elastic properties (E, ν). Application of (4.5) using the classical result from (3.3) for a plane strain crack of length b, $G_{ps} = (1-\nu^2)\pi\sigma^2 b/(2E)$, gives

$$\overline{G}_{ss} = \frac{\pi}{4}\frac{(1-\nu^2)}{E}\sigma^2 h \tag{4.12}$$

Note, again, that $\overline{G}_{ss} = \frac{1}{2}G_{ps}(h)$. Tunnel cracking cannot occur in a homogeneous material since plane strain spreading would take precedence over tunneling. Tunneling requires that the interface and toughness of the adjoining layers be sufficient to arrest crack advance at the layer interface.

Fig. 4.7 from Hutchinson and Suo (1992) extends (4.12) to the case of two equal finite thickness layers (#1) sandwiching the central layer (#2). The Dundurs parameters are again defined in (3.8). The limit $W \to \infty$ and $\alpha_D = \beta_D = 0$ corresponds to (4.12).

The elastic mismatch has a very large effect on $\overline{G}_{ss}$ when the central layer is relatively stiff.

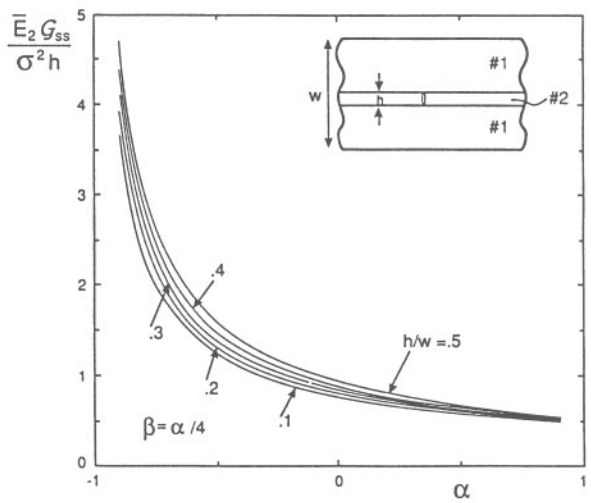

Fig. 4.7. Steady state energy release rate for a tunnel crack.

Combined effects accompanying tunnel cracking, such as debonding and sliding, contribute to the energy release rate, just as in the case of films. Some of these effects are discussed in detail in Evans and Hutchinson (1995).

5. DELAMINATION OF FILMS AND MULTILAYERS

Steady–state cracking is also central to the analysis of films and bilayers. Depending on the materials, geometry and stress states, delamination cracks can run on an interface or parallel to an interface in a brittle layer or substrate. The method outlined below is review in detail in Section III of Hutchinson and Suo (1992), which is the source of most of material presented in these notes. Original references are cited in that article.

5.1 Delamination of the Interface a Bilayer under Residual Stress

Consider the free–standing bilayer in Fig. 5.1 with residual stresses as determined in Section 2. (Note: the numbering here has the top layer as #1, not the bottom). In the uncracked, presented state, the residual stress distribution is equivalent to equal and opposite forces (per unit thickness in the out–of–plane direction) P and moments (per unit thickness) M_1 and M_2. The forces act through the mid points of the respective layers with the sign connection shown. By equilibrium,

$$M_1 + P(h + H)/2 = M_2 \tag{5.1}$$

For delamination along the interface, on the right in Fig. 5.1, the interface crack is shown advancing from the left edge of the bilayer. The bilayer is free–standing (unconstrained) and thus the resultant force and moment on each layer behind the crack tip is zero. As depicted in Fig. 5.1, the delamination problem is the sum of *prestressed state* plus the *reduced*

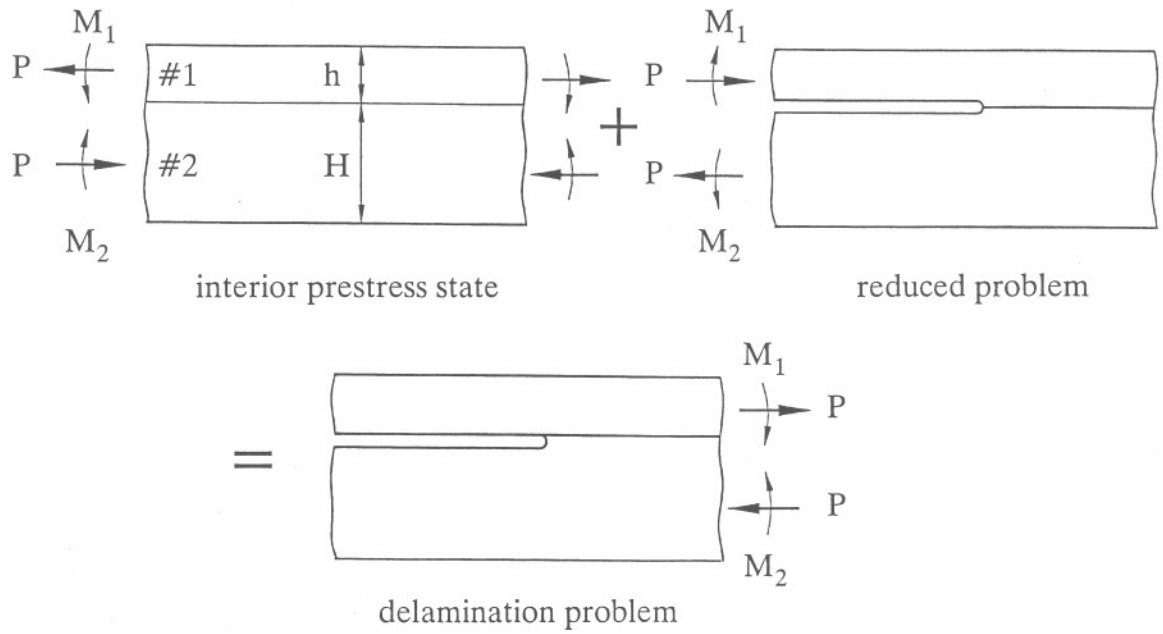

Fig. 5.1. Definition of reduced problem for interface delamination of free–standing, residually stressed bilayer. The reduced problem has the same G and ψ as the delamination problem. The forces and moments (per unit thickness out of the plane of the paper) are defined with the sense shown with the forces acting through the centers of the respective layers.

problem. The interface stress intensity factors of the delamination problem and the reduced problem are obviously the same. It is most convenient to use the reduced problem to determine the stress intensity factors and the energy release rate.

When the interface crack has penetrated well into the interior of the bilayer (i.e. at least several times h or H , whichever is smaller, from the edge), it attains steady–state such that G and ψ (or, equivalently, K_I and K_{II}) are independent of crack length. It is the steady–state solution which will be presented. As in the case of thin film cracking, the steady–state result can be used to determine a criterion which excludes interface delamination.

The steady–state energy release rate G for the reduced problem in Fig. 5.2 can be obtained by elementary means, as will be illustrated. The measure ψ of the relative proportion of K_{II} and K_I requires a complete elasticity analysis of the problem. The elastic mismatch is determined by the two Dundurs parameters (3.8). We begin by indicating the energy accounting which provides G .

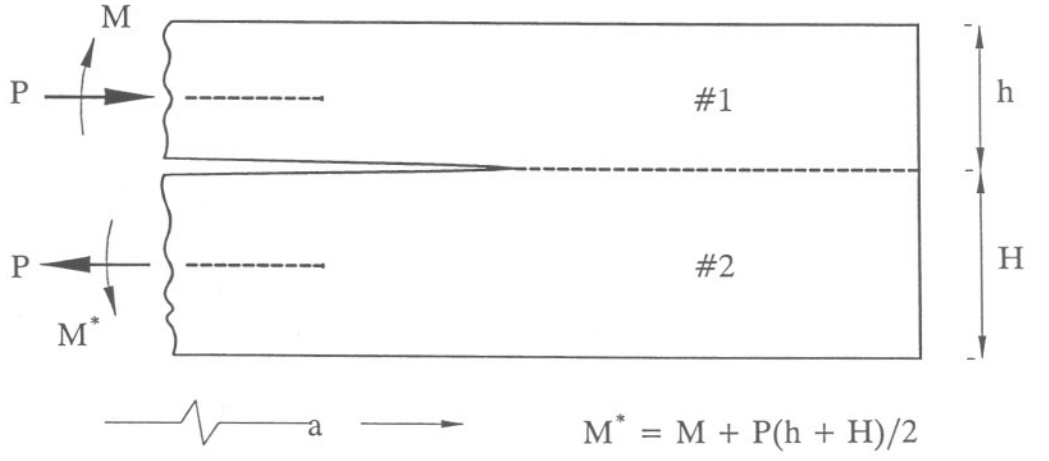

Fig. 5.2. Reduced problem for the bilayer.

Regard P and M as prescribed loads such that the potential energy per unit thickness of the system in Fig. 5.2, PE , is the elastic strain energy, SE , plus the potential energy of the loads. In the solution state, the potential energy of the loads is exactly $-2\,SE$, and thus at a given crack length a ,

$$PE(a) = -SE(a) \tag{5.2}$$

An energy accounting analogous to that made for steady–state film cracking is now made. Since,

$$G = -\frac{dPE}{da} = \frac{dSE(a)}{da} \tag{5.3}$$

the steady–state energy release rate, G_{ss}, can be obtained by taking the difference between the strain energy SED (per unit length per unit thickness) far ahead of the tip from that far behind the tip, i.e.

$$G_{ss} = (SED)_{DOWN} - (SED)_{UP} \tag{5.4}$$

Since $(SED)_{UP} = 0$, G_{ss} is just the sum of strain energy in the two beam arms far down behind the tip (per unit thickness per unit length). This can be computed *rigorously* using beam theory. The result is straightforward but algebraically a bit messy. It is given in Section III.B.4 of the article of Hutchinson and Suo (1992) and on page 2519 of the article by Evans and Hutchinson (1995).

The determination of $\psi = \tan^{-1}(K_{II}/K_I)$ requires solution of the elasticity problem posed by Fig. 5.2. The general solution to this problem has been obtained (using numerical solution of an integral equation formulation), and the results (with basic references) are presented in Section III.B.4 of the article cited above. The elastic mismatch is captured for this problem by dependencies on the Dundurs parameters. For $\beta_D = 0$, the solution has the form

$$\begin{aligned} K_I &= c_{11} P h^{-1/2} + c_{12} M h^{-3/2} \\ K_{II} &= c_{21} P h^{-1/2} + c_{22} M h^{-3/2} \end{aligned} \tag{5.5}$$

where the c_{ij}'s depend on α_D and h/H. A limiting case of some interest for thin film applications is $h/H \to 0$, i.e. the thin film on a deep substrate. For example, the reduced problem with $M = 0$ in Fig. 5.3, is relevant to delamination of a film under uniform *tension*, with $P = \sigma h$.

For general combinations of P and M the solution to the problem in Fig. 5.3 is

$$\begin{aligned} K_I &= \frac{1}{\sqrt{2}}\left[P h^{-1/2} \cos\omega + 2\sqrt{3}\, M h^{-3/2} \sin\omega\right] \\ K_{II} &= \frac{1}{\sqrt{2}}\left[P h^{-1/2} \sin\omega - 2\sqrt{3}\, M h^{-3/2} \cos\omega\right] \end{aligned} \tag{5.6a}$$

where $\omega(\alpha_D)$ is plotted in Fig. 3.4. When $\alpha_D = 0$, $\omega = 52.07^\circ$. The energy release rate is

$$G = \frac{\left(1 - \nu_1^2\right)}{E_1 h^3}\left[\frac{1}{2} h^2 P^2 + 6M^2\right] \tag{5.6b}$$

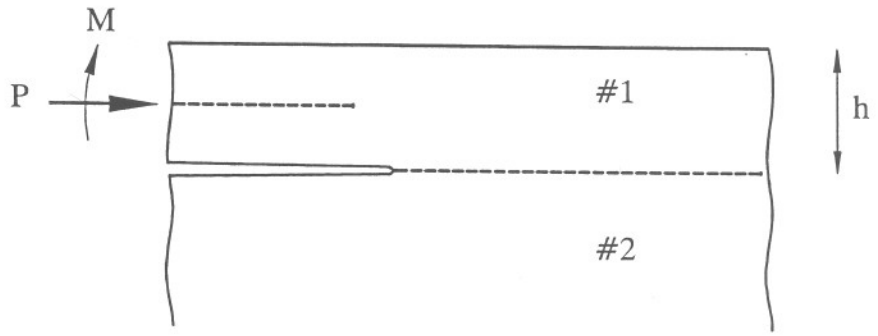

Fig. 5.3. Reduced problem for a thin film on an infinite substrate. P and M are related to the through–thickness stress distribution $\sigma(z)$ in the film by

$$P = \int_0^h \sigma(z)dz \text{ and } M = \int_0^h \sigma(z)(z - h/2)dz .$$

Note, for example, if $M = 0$, then $K_I > 0$ when $P > 0$, and conversely. The solution (5.6) is only valid in the range of P and M where $K_I > 0$, i.e. a open crack.

The criterion which excludes steady–state interface delamination is

$$G_{ss} < \Gamma_c(\psi) \tag{5.7}$$

As in the case of film cracking, this can be cast in the form of (1.1). For the thin film on the deep substrate the requirement is

$$\frac{\left(1 - \nu_1^2\right)\sigma^2 h}{E_1 \Gamma_c(\psi)} < 2 \tag{5.8}$$

If $\sigma > 0$, $\psi = \omega(\alpha_D)$, as plotted in Fig. 3.4. If $\sigma < 0$ (a film under compression), (5.8) still applies, but (5.6) predicts that $K_I < 0$, which indicates that the crack is closed with $K_I = 0$. In this case the crack is in pure mode II with $\psi = -90^\circ$. The proviso for (5.8) in this case is that the friction force between the film and the substrate can be neglected. Otherwise, (5.8) is overly conservative.

5.2 Delamination of a Bilayer by Layer Cracking Parallel to the Interface

It is not uncommon for a metal film under residual tenson when bonded to a ceramic substrate to drive a delamination crack in the substrate well below the interface. The crack parallels the interface, and a steady–state situation again prevails. Since the substrate is homogeneous, a necessary requirement is that the crack be positioned such that $K_{II} = 0$. The general reduced problem for sub–interface delamination is indicated in Fig. 5.4. The arguments made in the previous sub–section for determining G_{ss} apply here as well, and general results are given in the same references cited. Full characterization of this solution, which now depends on h/d as well as α_D, β_D and h/H, is available in the original reference cited.

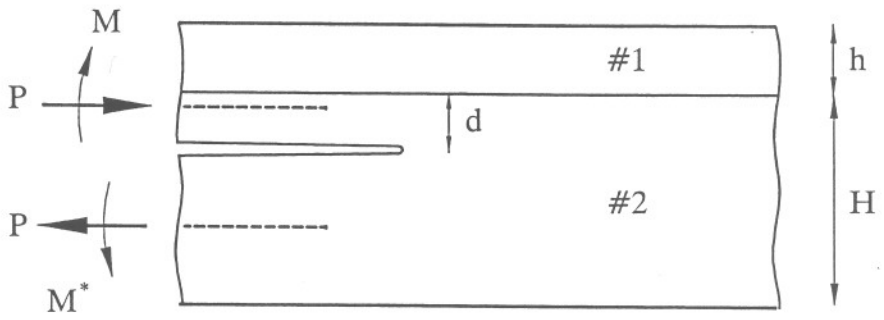

Fig. 5.4. The reduced problem for sub–interface cracking of a bilayer. The force P is taken to act in the direction shown through the respective neutral bending plane of each arm.

Substrate delamination can be illustrated by considering a film carrying a uniform residual tension σ bonded to an infinitely thick substrate, where there is *no elastic mismatch*. In this case, the solution (5.6) with $\omega = 52.07^{o}$ is applicable. The solution for a crack at an arbitrary depth d below the interface is obtained with the help of Fig. 5.5. For a uniformly stresses thin film in the tension σ, the reduced problem is given in Fig. 5.5a. In the absence of elastic mismatch (i.e. $\alpha_D = \beta_D = 0$), the reduced problem is equivalent to that shown in Fig. 5.5b. Therefore, by (5.6), with $h \rightarrow (h + d)$,

$$K_{II} = \frac{(\sigma h)}{\sqrt{2(h + d)}}\left[\sin\omega - \sqrt{3}\frac{d}{h + d}\cos\omega\right] \tag{5.9}$$

Imposing $K_{II} = 0$ gives as the depth of the delamination crack below the interface

$$\frac{d}{h + d} = \frac{1}{\sqrt{3}}\tan\omega = 0.741 \quad \text{or} \quad \frac{d}{h} = 2.86 \tag{5.10}$$

The associated values of K_I and G_{ss} from the first equation in (5.6) are

$$K_I = \frac{(\sigma h)}{\sqrt{2(h + d)}}\left[\frac{1}{\cos\omega}\right] = 0.586\,\sigma\sqrt{h} \tag{5.11a}$$

$$G_{ss} = \frac{1 - \nu^2}{E}K_I^2 = 0.343\frac{(1 - \nu^2)}{E}\sigma^2 h \tag{5.11b}$$

Note that G_{ss} for sub–interface cracking is only 31% below the corresponding value (3.12) for interface cracking.

The condition for excluding substrate delamination in this case is

$$\frac{(1 - \nu^2)\sigma^2 h}{E\Gamma_c^{(2)}} < 2.93 \tag{5.12}$$

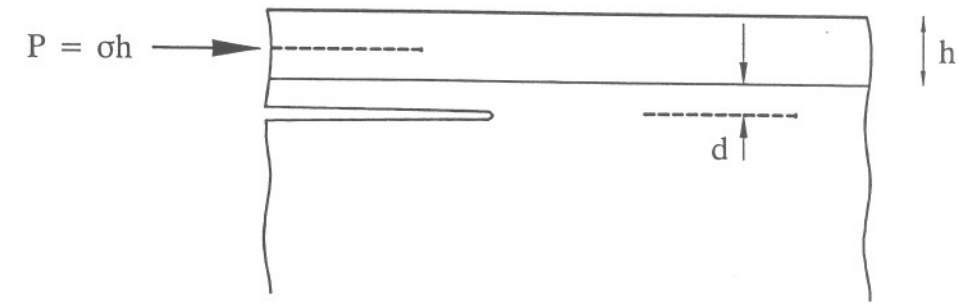

a)

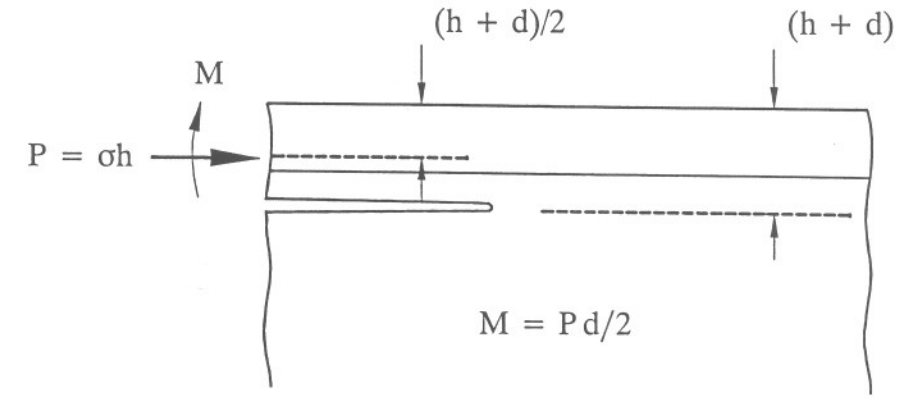

b)

Fig. 5.5. (a) Reduced problem for sub–interface delamination for a film under residual tension σ. (b) Equivalent reduced problem when there is no elastic mismatch. Now (5.6) applies but with h replaced by h + d.

where $\Gamma_c^{(2)}$ is the mode I substitute toughness. If the residual stress in the film is *uniform compression*, the only potential mode I crack location in the substrate is still given by (5.10), but it is associated with *negative* K_I, implying that the crack is closed and (5.6) is not valid. The conclusion to be drawn is that substrate delamination is not possible when the film is under uniform compression.

5.3 Interface and Layer Delamination for Multilayers

The equations for the steady–state energy release rate for either an interface crack or a inter–layer crack parallel to the interfaces are readily obtained using the energy accounting scheme laid out in Section 5.1. The equations though elementary require numerical evaluation, which is best done by a computer program. General results for the mode measure ψ are not available for other than bilayers and certain trilayers. Approximations for ψ can be had by replacing the layers above and below the crack equivalent homogeneous layers and then using the general bilayer results. This procedure is also best implemented in a small computer program. Software for making calculations of G_{ss} and ψ for cracks in arbitrary locations (both tunneling and delamination) is available from A.G. Evans and J.W. Hutchinson.

6. BUCKLING DRIVEN DELAMINATION FOR THIN FILMS UNDER RESIDUAL COMPRESSION

Thin films under uniform equi–biaxial compression, $\sigma_{11} = \sigma_{22} = -\sigma$, are considered. The two main failure modes are edge delamination governed by (5.8) and buckling driven delamination. The approach to buckling driven delamination of thin films is taken from Section VI of the review article by Hutchinson and Suo (1992) and a more recent publication by Hutchinson, Thouless and Liniger (1992). The most recent comprehensive articles on the subject are by Ortiz and Gioia (1994) and Gioia and Ortiz (1996).

If an initially debonded interface region exists in the interior of the film/substrate interface, that region will buckle away from the substrate if the residual film stress is large enough. *Prior to buckling* there is no stress intensity at the edge of the interface crack. Once the film buckles, however, elastic energy stored in the film is released and the interface crack is subject to mixed mode conditions governed by G and ψ. If the stress is sufficiently large, or, equivalently, if the initially debonded region is large enough, interface crack growth will occur and the blister will spread. It will be seen that the dependence of interface toughness on the mixed mode measure ψ is essentially to understanding buckle driven delamination. Without the strong mode dependence discussed in connection with Fig. 3.5, a blister would completely delaminate the film once it started to spread. The highly unusual morphologies displayed by buckling delaminations (e.g. "telephone cord" blisters, wiggly circular blisters, straight–sided blisters) would not exist without mode–dependent interface toughness $\Gamma_c(\psi)$.

The contents of Section 6 are:

(6.1) Straight–sided blisters.

(6.2) Circular blisters.

(6.3) Propagation of straight vs. curved blister boundaries and hints on the curious shapes of buckled blisters.

6.1 Straight–sided Blisters

With reference to Fig. 6.1, consider a thin film on an infinitely deep substrate which has a debonded region on the interface specified by $|y| \le b$ and $|x| < \infty$. We focus on conditions on the straight sides of the debonded region along $y = \pm b$. When the film is unbuckled, the stress in the film is everywhere equi–biaxial compression σ. There are no tractions on the interface and $G = 0$. If film buckles up from the substrate, the compression in the film near the edge at $y = b$ is partially relieved and a moment M (per unit

length in the x−direction) develops. Denote the stress release averaged through the film thickness by ΔN (force per unit length in the x−direction) with the positive sense shown in Fig. 6.1. The energy release rate G and the mode mixity ψ along the edge of the buckled blister can be determined from (5.6) if ΔN and M are known. A straightforward derivation of M and ΔN at the blister edge are now obtained using plate theory to represent the buckled film.

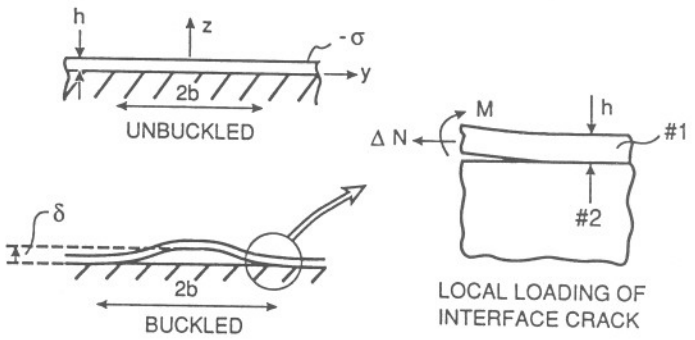

Fig. 6.1. Geometry of the straight−sided blister, and conventions for the elasticity solutions characterizing conditions along the straight edge of the interface crack.

The auxilary buckling problem is shown in Fig. 6.2. A wide plate (infinite in extent in the x−direction) is clamped along its edges and subject to edge compression T (force/length). If this piece of the film were cut away from the substrate and unloaded along its edges it would have a width $2b(1 + \epsilon)$ where

$$\epsilon = \frac{1 - \nu_1^2}{E_1}\sigma \tag{6.1}$$

(Plane strain is applicable such that the strain change in the x−direction is zero. Thus, the plane strain tensile modulus appears above). The plate in the upper figure in Fig. 6.2 must be squeezed back to length $2b$ for it to "fit" back in place on the substrate.

The solution to the auxilary plate buckling problem in Fig. 6.2 is elementary. The deflection $w(y)$ must satisfy

$$Dw'''' + Tw'' = 0 \;\; ; \;\; w = w' = 0 \;\; \text{at} \;\; y = \pm\, b \tag{6.2}$$

where $D = E_1 h^3/\left[12(1 - \nu_1^2)\right]$. (This equation, although linear in w, is exactly what is obtained without approximation from the fully nonlinear von Karman plate equations).The solution is as follows. For $T < T_c$, where

$$T_c = \frac{\pi^2}{12}\frac{E_1 h}{\left(1 - \nu_1^2\right)}\left(\frac{h}{b}\right)^2 \tag{6.3}$$

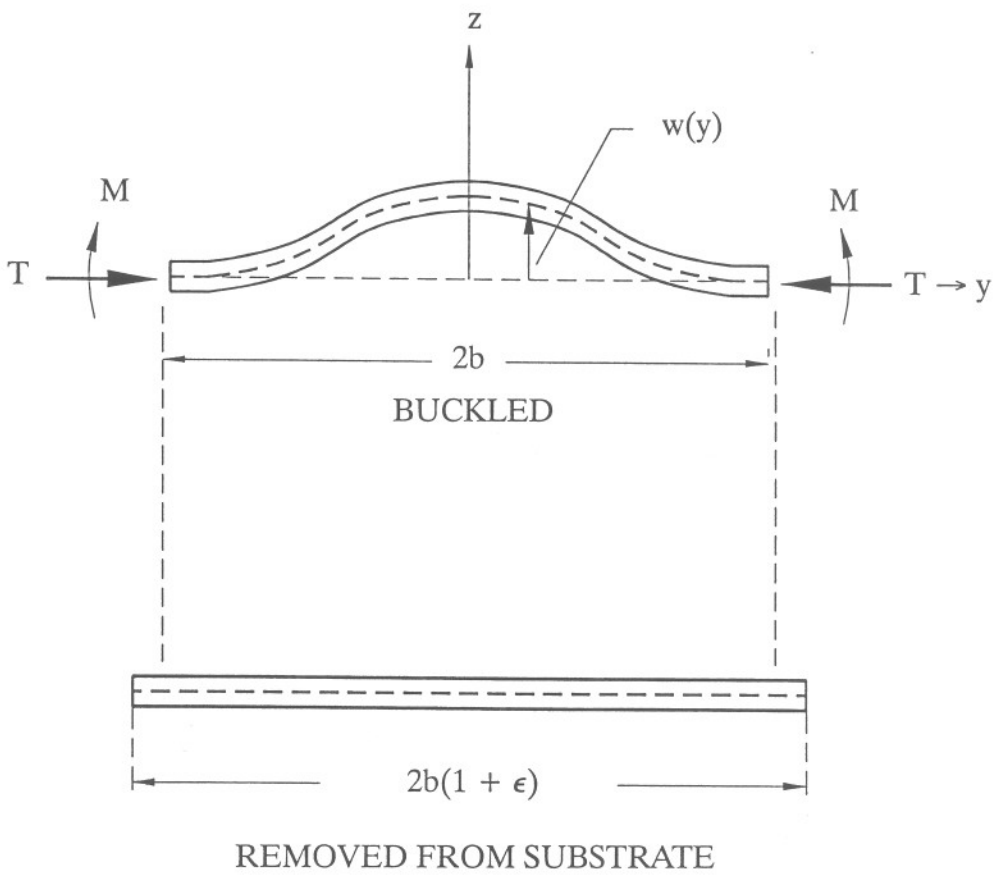

Fig. 6.2. Auxilary problem for determining ΔN and M.

the plate is unbuckled. For $T = T_c$, buckled solutions exist given by

$$w(y) = \frac{1}{2}\delta[1 + \cos(\pi y/b)] \tag{6.4a}$$

where δ is the buckling deflection at $y = 0$. A wide plate can experience any amplitude of buckling when $T = T_c$ according to nonlinear plate theory. The *shortening* of the plate relative to its unstressed length $2b(1 + \epsilon)$ is

$$\Delta L = \frac{2b\left(1 - \nu_1^2\right)T_c}{E_1 h} + \frac{1}{2}\int_{-b}^{b} w'^2 dy$$

$$= \frac{2b\left(1 - \nu_1^2\right)T_c}{E_1 h} + \frac{\pi^2}{8b}\delta^2 \tag{6.4b}$$

The auxilary solution is now employed to determine ΔN and M defined in Fig. 6.1. For the auxilary plate to fit back in place, we must impose $\Delta L = 2b\epsilon$ where ϵ is given by (6.1). By (6.4b) this requires

$$\delta^2 = \frac{16b^2}{\pi^2}\frac{\left(1-\nu_1^2\right)}{E_1}(\sigma - \sigma_c) \tag{6.5}$$

where

$$\sigma_c = \frac{T_c}{h} = \frac{\pi^2}{12}\frac{E_1}{\left(1-\nu_1^2\right)}\left(\frac{h}{b}\right)^2 \tag{6.6}$$

If $\sigma < \sigma_c$, the film is *unbuckled* and (6.5) does not apply. If $\sigma > \sigma_c$, then, from $M = Dw''$ at $y = b$,

$$M = \frac{\pi^2\delta}{2b^2} = \frac{1}{2}\sigma_c h^2\left(\frac{\delta}{h}\right) \tag{6.7}$$

The released edge force defined as the *change* due to buckling – it is only the change which contributes to the interface stress intensities – is given by $\Delta N = (\sigma - \sigma_c)h$.

Finally, identify ΔN with $-P$ in the solution (5.6) for the problem in Fig. 5.3. Straightforward algebraic reduction gives for $\sigma \geq \sigma_c$

$$G = \frac{\left(1-\nu_1^2\right)h}{2E_1}(\sigma - \sigma_c)(\sigma + 3\sigma_c) \tag{6.8}$$

and

$$\tan\psi = \frac{4 + \sqrt{3}\,\xi\tan\omega}{-4\tan\omega + \sqrt{3}\,\xi} \tag{6.9}$$

where

$$\xi \equiv \frac{\delta}{h} = \left[\frac{4}{3}\left(\frac{\sigma}{\sigma_c} - 1\right)\right]^{1/2} \tag{6.10}$$

Note that for $\sigma >> \sigma_c$,

$$G \to G_0 = \frac{\left(1-\nu_1^2\right)h\sigma^2}{2E_1} \tag{6.11}$$

which is the result for edge–delamination.

Plots of G/G_0 and ψ as functions of σ/σ_c are given in Fig. 6.3. The energy release rate attains a maximum $4G_0/3$ at $\sigma/\sigma_c = 3$, and then slowly decays to G_0. More significantly,

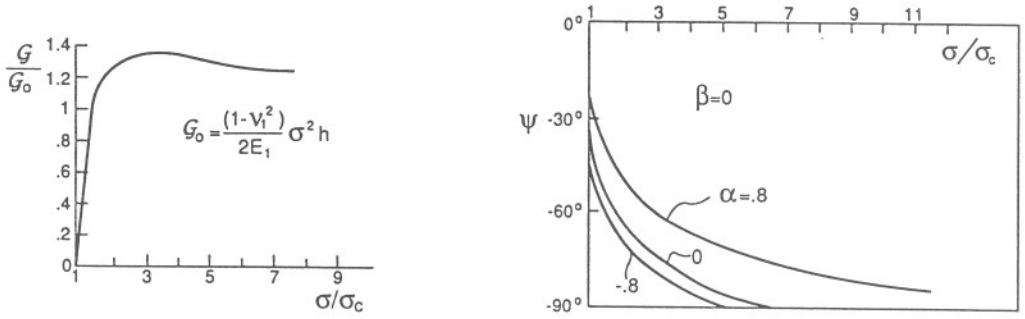

Fig. 6.3. G and ψ along the edges of a straight–sided blister. σ_c and G_0 are given by (6.6) and (6.11).

the mode mixity ψ become dominately mode II as σ/σ_c increases. At the onset of buckling when σ/σ_c is only slightly above unity, the interface experiences a higher proportion of mode I to mode II. Given the strong mixed mode dependence of the toughness of many interfaces, $\Gamma_c(\psi)$, the ψ–dependence in Fig. 6.3 implies that a spreading blister will encounter increased resistance to propagation due to increasing interface toughness. Before pursuing this further, the corresponding results for circular blisters will be presented.

6.2 Circular Blisters

The scheme for determining G and ψ for a circular blister of radius R is similar to that discussed above. An important difference is that the auxilary buckling problem for the circular plate is nonlinear in the deflection. It must be solved numerically. Details are presented in Hutchinson, Thouless and Liniger (1992). Plots of G and ψ are given in Fig. 6.4 where now

$$G_0 = \frac{(1-\nu_1)h\sigma^2}{E_1} \tag{6.12}$$

and

$$\sigma_c = 1.2235\frac{E_1}{1-\nu_1^2}\left(\frac{h}{R}\right)^2 \tag{6.13}$$

Note that G_0 is the elastic energy per unit area stored in the biaxially stressed film in the unbuckled state. Qualitatively, the trends for the circular blister are similar to those for the straight–sided blister. However, G increases monotonically with increasing σ/σ_c^*, and ψ approaches mode II more gradually than for the straight–sided blister. This later distinction will emerge as important in understanding blister morphologies.

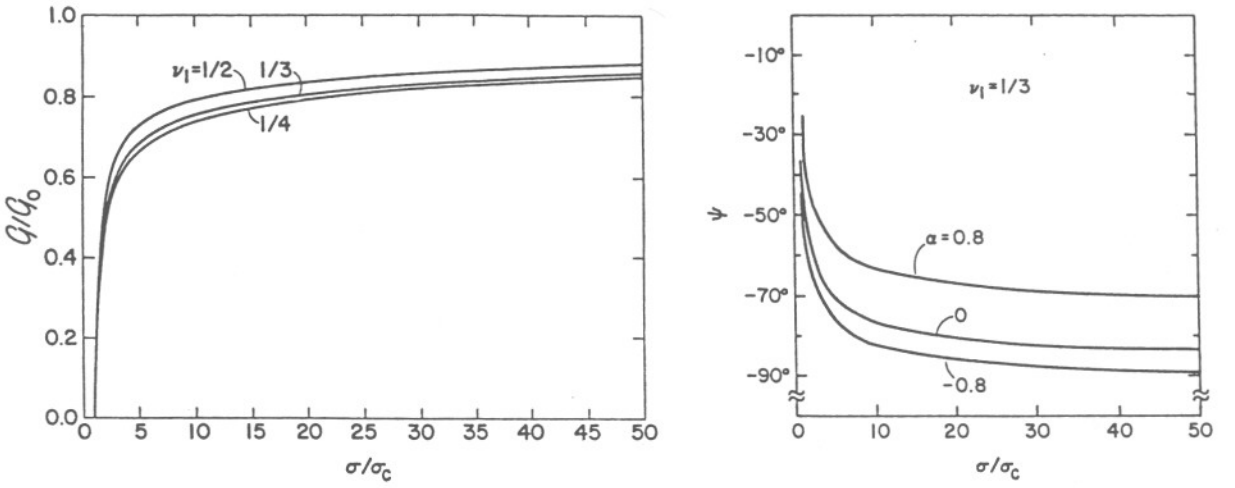

Fig. 6.4. G and ψ for a circular blister. σ_c and G_0 are defined in (6.13) and (6.12).

6.3 Propagation of Straight vs. Curved Blister Boundaries and Hints on the Curious Shapes of Buckled Blisters

For a given initial blister size, G increases with increasing σ until

$$G = \Gamma_c(\psi) \tag{6.14}$$

at which point the blister will begin to spread. As the size, b or R, increases σ_c decreases. The *combined effect* of increasing σ and increasing size is felt through the variable σ/σ_c. Because $|\psi|$ increases as σ/σ_c increases, the energy release rate at the crack edge (6.14) must increase for interfaces which are tougher in mode II than mode I. It is useful for the purpose of discussion to introduce a specific interface toughness function and a mode–adjusted crack driving force.

Following Hutchinson, *et al.* (1992), let

$$\Gamma_c(\psi) = \Gamma_{Ic} f(\psi) \tag{6.15a}$$

where Γ_{Ic} is the mode I interface toughness and

$$f(\psi) = 1 + \tan^2[(1 - \lambda)\psi] \tag{6.15b}$$

Plots of $f(\psi)$ for various λ are given in Fig. 6.5, along with the ratio of the mode II to mode I toughnesses as dependent on λ. If $\lambda = 1$, the interface toughness has no mode–dependence. The limit $\lambda = 0$ corresponds to the criterion $K_I = K_{Ic}$ for all combinations of K_I and K_{II}. Values of λ between 0.1 and 0.3 appear to capture trends for some of the interface toughness data sets available.

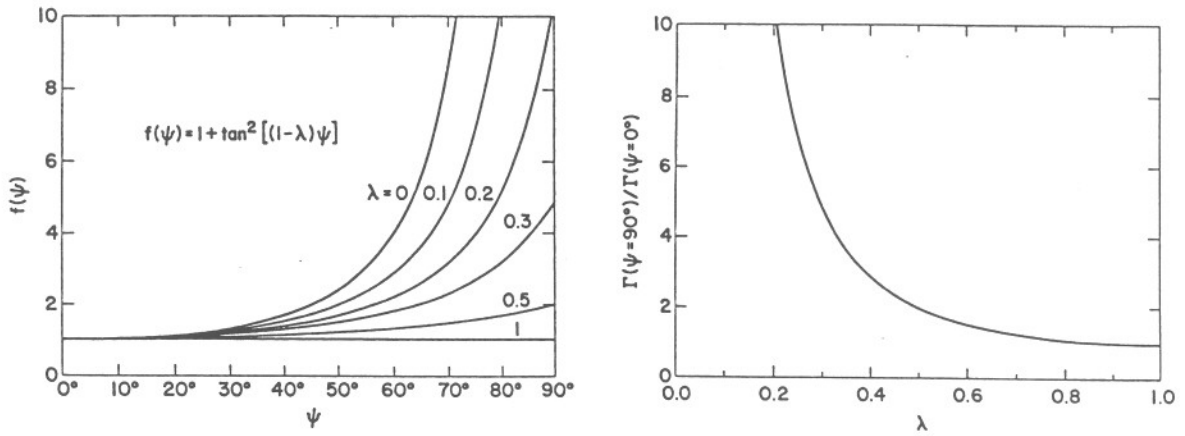

Fig. 6.5. Mode dependence function $f(\psi)$ and ratio of mode II to mode I toughnesses as dependent on λ.

Define a *mode–adjusted crack driving force* $\mathcal{F}$ by

$$\mathcal{F} = G/f(\psi) \tag{6.16}$$

So that by (6.15a) the crack advance criterion (6.14) becomes

$$\mathcal{F} = \Gamma_{Ic} \tag{6.17}$$

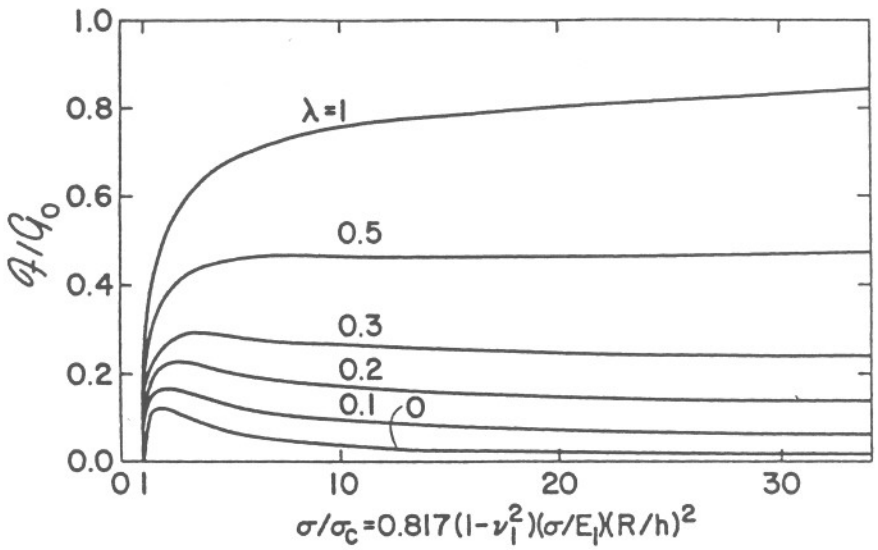

Fig. 6.6. Mode–adjusted crack driving force for circular blister $\nu_1 = 1/3$ and $\alpha_D = 0$.

Plots of $\mathcal{F}$ vs. σ/σ_c for the circular blister are given in Fig. 6.6 for various λ. For all cases with $\lambda < .5$, $\mathcal{F}$ *decreases* after σ/σ_c has exceed about 2. This implies that σ must be increased if the blister is to spread once σ/σ_c has exceeded about 2. This is seen most clearly in Fig. 6.7 where the condition (6.17) has been imposed on the solution. For $\lambda \geq .5$, the blister will *spread spontaneously without arrest* once it becomes critical. For $\lambda < .5$ spreading requires *increasing* σ once the blister has reached a condition where $\sigma/\sigma_c > 2$. Note that the condition for spreading can be written as

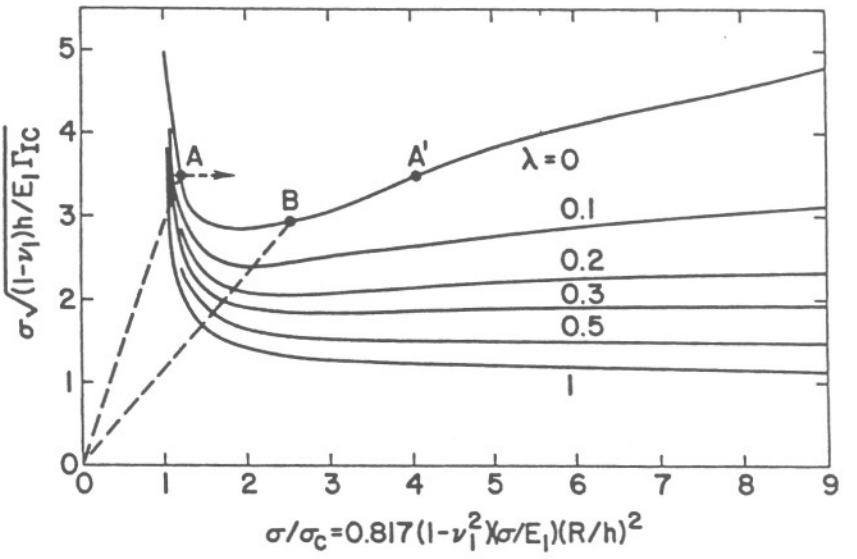

Fig. 6.7. Normalized stress from imposition of $G = \Gamma_c(\psi)$ (or $\mathcal{F} = \Gamma_{Ic}$) for spread of a circular blister with $\nu_1 = 1/3$ and $\alpha_D = 0$.

$$\frac{\left(1 - \nu_1^2\right)\sigma^2 h}{E_1 \Gamma_{Ic}} > \Omega_c(\lambda) \tag{6.18}$$

where Ω_c lies between about 4 and 9 for λ between 0 and 0.3.

As shown on the left in Fig. 6.8, a straight–sided blister propagates by interface crack growth at its curved end rather than along its straight sides. To gain some insight into the tendency for blisters to advance at regions of high curvature along the interface crack boundary, we compare the mode–adjusted crack driving force $\mathcal{F}$ for circular blisters with those for straight–side blisters. Using the definition in (6.16) with (6.15b), $\mathcal{F}$ is determined

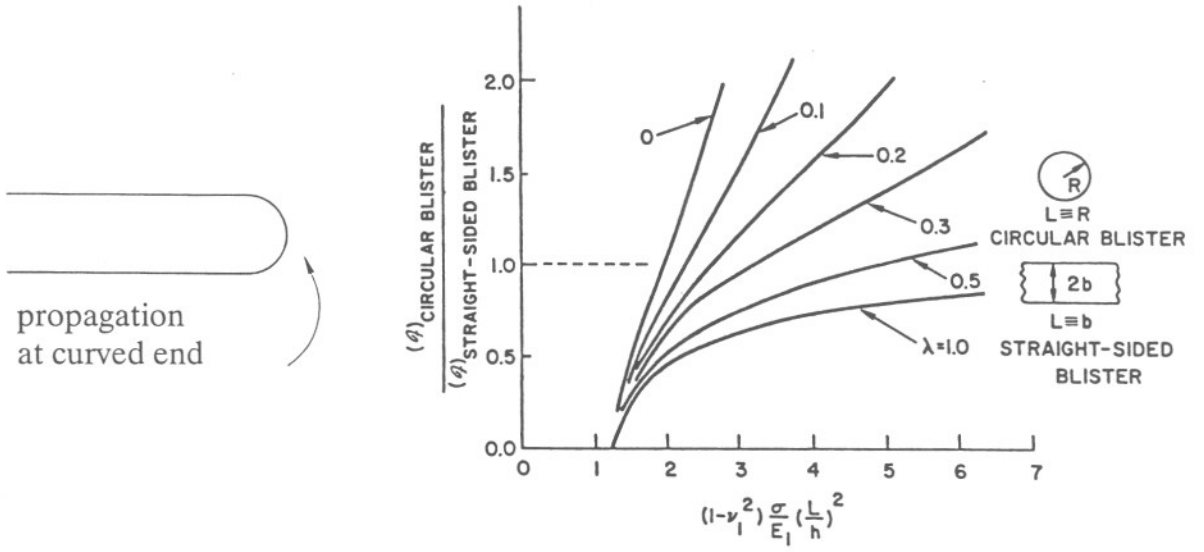

Fig. 6.8. Ratio of mode–adjusted crack driving force for a circular blister to that for a straight edge of the straight–sided blister. The comparisons are made with R = b and at the same level of equi–biaxial compression σ.

from (6.8) and (6.9) for the straight edge and, as above, using the result from Fig. 6.4 for the circular blister. As indicated in Fig. 6.8, the $\mathcal{F}$–values for the two blisters are compared at sizes such that $L = 2b = 2R$.

If $\lambda = 1$ (mode independent interface toughness), the straight edge has the greatest crack driving force and would be most likely to be observed. Recall that when $\lambda = 1$, the blister would spread without arrest in any case. For $\lambda \leq 0.3$, the curved boundary has the largest crack driving force once

$$\left(1 - \nu_1^2\right)\frac{\sigma}{E_1}\left(\frac{L}{h}\right)^2 \tag{6.19}$$

has exceed a value between 2 and 3, depending on λ. This suggest that crack advance is most likely on curved crack fronts once the parameter (6.19) attains a critical level. The qualitative conclusion emerging from the examples discussed in this section is that the unusual shapes of blisters arise from their tendency to grow towards mode II conditions, coupled with a strong mode dependence of interface toughness. Efforts to predict the evolution of the telephone cord blister have been only partically successful. Some aspects are detailed in the review article by Gioia and Ortiz (1996). Results for the propagation of the straight–sided blister are given in the Hutchinson and Suo article (1992), and comparisons between theory and experiment on wavy–edged circular blisters are included in the paper by Hutchinson, Thouless and Liniger (1992).

References

Original references are cited in the articles by Hutchinson and Suo (1992) and Evans and Hutchinson (1995). The references listed alphabetical below are unlisted in these references and/or published subsequently.

Beuth, J.L. (1992) "Cracking of thin bonded films in residual tension", Int. J. Solids Structures **29**, 1657–1675.

Beuth, J.L. and Klingbeil, N.W. (1996) "Cracking of thin films bonded to elastic–plastic substrates", J. Mech. Phys. Solids **44**, 1411–1428.

Evans, A.G. and Hutchinson, J.W. (1995) "The thermomechanical integrity of thin films and multilayers", Acta Metall. Mater. **43**, 2507–2530.

Freund, L.B. and Hu (1988) unpublished report on stress transfer from film to substrate.

Gioia, G. and Ortiz, M. (1996) "Delamination of compressed thin films", to be published in Advances in Applied Mechanics **33**, (Eds. J.W. Hutchinson and T. Wu).

He, M.Y., Evans, A.G. and Hutchinson, J.W. (1994) "Crack deflection at an interface between dissimilar elastic materials: role of residual stresses", Int. J. Solids Structures **31**, 3443–3455.

Hutchinson, J.W. and Suo, Z. (1992) "Mixed mode cracking in layered materials", in Advances in Applied Mechanics **29**, (Eds. J.W. Hutchinson and T. Wu), 63–191.

Hutchinson, J.W., Thouless, M.D. and Liniger, E.G. (1992) "Growth and configurational stability of circular, buckling–driven film delaminations", Acta Metall. Mater. **40**, 295–308.

Liechti, K.M. and Chai (1992) "Asymmetric shielding in interfacial fracture under in–plane shear", J. Appl. Mech. **59**, 295–304.

Murakami, Y. (1987) Stress Intensity Factors Handbook, Pergamon Press.

Nakamura, T. and Kamath, S. (1992) "Three–dimensional effects in thin film fracture", Mech. Materials **13**, 67–77.

Ortiz, M. and Gioia, G. (1994) "The morphology and folding patterns of buckling–driven thin–film blisters", J. Mech. Phys. Solids **42**, 531–559.

Tada, H., Paris, P.C. and Irwin, G. (1985) Stress Analysis of Cracks Handbook, published by Del Research.